# TWO-PHOTON POLYMERIZATION 4D PRINTING OF MECHANICAL METAMATERIALS

AYMAN AHMED MUBEEN

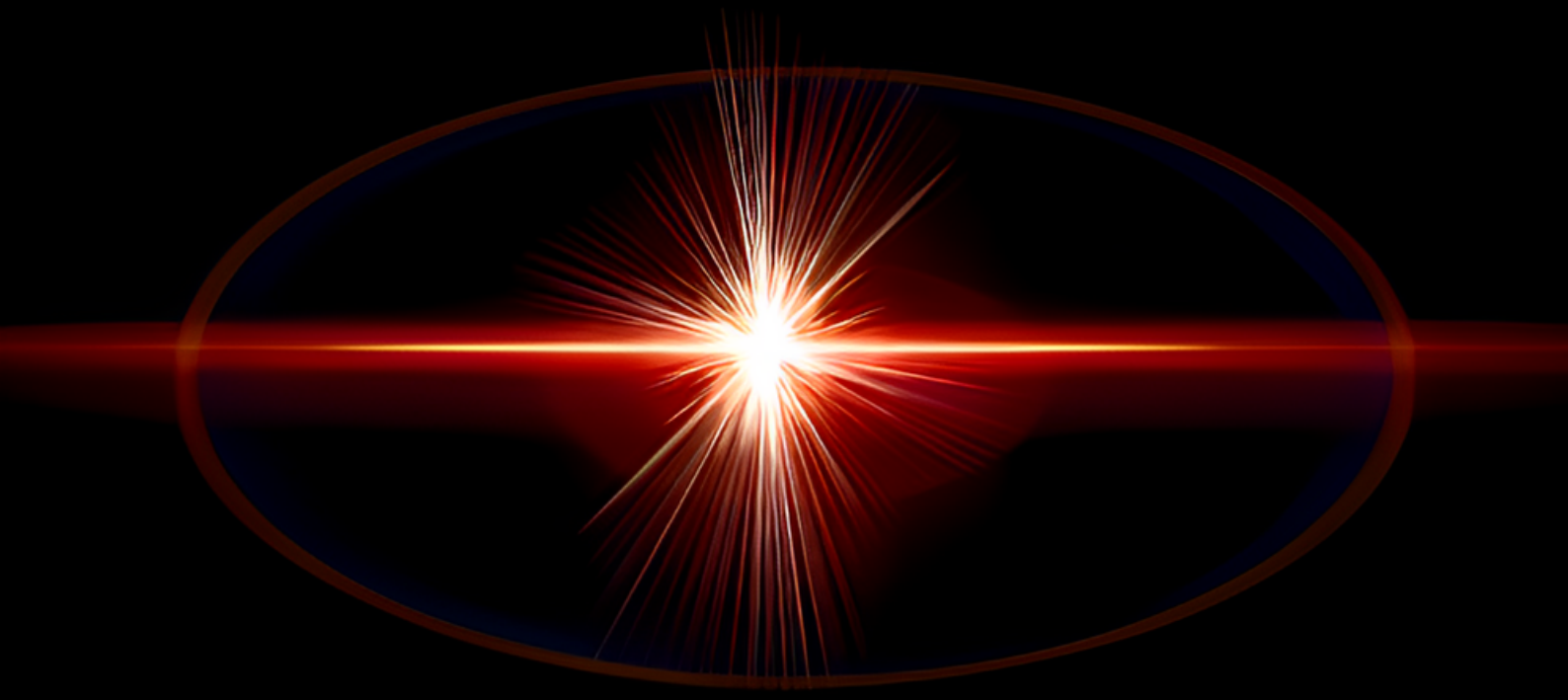

TU Delft

# Two-Photon Polymerization 4D Printing of Mechanical Metamaterials

by

Ayman Ahmed Mubeen

In partial fulfillment of the requirements for the degree of

**Master of Science**

In Mechanical Engineering

At Delft University of Technology,

To be defended on August 31, 2023, at 10:30.


| | |
|---|---|
| **Supervisors :** | Dr. Mohammad J. Mirzaali, Dr. Angelo Accardo |
| **Daily Supervisor :** | Ebrahim Yarali (PhD) |
| **External committee member :** | Dr. Andres Hunt |
| **Project Duration :** | November, 2022 - August, 2023 |
| **Student Number :** | 5520908 |
| **Faculty :** | Mechanical, Maritime, and Materials Engineering (3ME), TU Delft |


An electronic version of this thesis is available at `http://repository.tudelft.nl/`
(The thesis is under embargo until July 2028)

TU Delft

# Overiew

This research work titled "Two-Photon Polymerization 4D Printing of Mechanical Metamaterials" brings together the realms of engineering design, chemistry, material science, and micro and nano engineering. This work was a collaborative effort by the 'Biomaterials Department' and the 'Precision Microsystems Engineering Department' at TU Delft, and delves into the domain of micro-4D printing, with an aim of creating dynamic engineered microstructures capable of interacting with cellular microenvironments in a more natural manner.

The project commenced in November 2022, with a literature survey phase. An exhaustive review was conducted to acquire insights into the already existing literature, and find areas where potential contributions could be made. The literature survey culminated with forming the research question, which was centered around integrating 4D printing into the field of metamaterials to develop dynamic metamaterial-based microstructures capable of exhibiting a varying Poisson's ratio, with potential applications in the field of tissue engineering.

Over the course of the next 6 months that followed, mechanical designs for the proposed structures were developed, followed by fabrication using a state-of-the-art two-photon polymerization-based microfabrication technique. Numerous characterizations were performed to evaluate and fine-tune the performance of the microstructures, before finally arriving at a design that met all the desired requirements. The project concluded with successfully fabricating and testing a metamaterial-based microstructure capable of exhibiting a dynamic and reversible response when subjected to an external stimulus. Though numerous improvements still have to be made before the microstructures can actually be implemented for cell culture applications, this research marks a significant step towards achieving the target of a stimuli-responsive metamaterial-based 3D scaffold for tissue engineering applications. Furthermore, this research work lays the groundwork for many more promising projects in this field.

Our research findings are presented in the form of a scientific paper, and elaborate descriptions of some of the key concepts are provided in the appendix. I hope the paper presented will offer readers a comprehensive insight into our research, and a glimpse of our vision for the future of tissue engineering.

# Acknowledgements

This thesis project is the culmination of my Master's in Mechanical Engineering at Delft University of Technology, and has been a challenging yet incredibly rewarding journey. The thesis marks the completion of my academic pursuits, and I am immensely grateful for the support and guidance I have received throughout this endeavor. First and foremost, I would like to thank my parents for giving me the freedom to follow my dreams, and for supporting me in every possible way. Their understanding and encouragement have always been a constant source of strength and motivation.

I would like to extent my heartfelt gratitude to my supervisors Dr. Mohammad J. Mirzaali and Dr. Angelo Accardo. Dr. Mohammad gave me this opportunity, and his expertise, ideas, and guidance provided me with an excellent direction for my thesis. I would like to sincerely thank Dr. Angelo for his expertise, unwavering support, care, and for ensuring that I stayed on track during my thesis. The faith and confidence my supervisors expressed in me and my work served as a constant source of motivation throughout the duration of my thesis. I extend my sincere appreciation to my daily supervisor, Ebrahim Yarali. This project would not have been possible without your mentorship, guidance, enthusiasm for the topic, and constant encouragement. Your insightful feedback and thought-provoking discussions pushed me to be a better version of myself. It was a pleasure working alongside you.

Special thanks go to the individuals from the two research groups I have had the privilege of being a part of. From the Biomaterials group, I would like to thank Lennart, Mauricio, Vahid, Pier, kai, Jason, and Nasim for their feedback during the weekly group meetings. It truly contributed to making my thesis better. From the MNE group, my foremost gratitude extends to Ahmed Sharaf for training me on using the Nanoscribe, and patiently addressing all my doubts. It was a joy working with you. I would also like to thank Pieter, Francesco, Nastaran, Vijay, George, and Himanshu for their practical insights during my project, and the interesting conversations at the Nanoscribe lab.

Lastly, through the course of my Master's program, I have had the privilege of meeting some interesting people who added much value to my life. The time I have spent with my roommates and friends has made this journey truly memorable. I am immensely grateful for these wonderful experiences.

*Ayman Ahmed Mubeen*
*Delft, August 2023*

CONTENTS

# Two-Photon Polymerization 4D Printing of Mechanical Metamaterials

Ayman Ahmed Mubeen
Master Thesis, TU Delft

***Abstract*—Shape morphing is a prevalent feature in all living organisms. Incorporating shape-morphing capabilities into engineered scaffolds in the field of tissue engineering by virtue of 4D printing would allow for structures to closely mimic in-vivo conditions, and dynamically interact with changing cellular microenvironments. Engineered scaffolds subjected to external mechanical loads have recently drawn interest to study the impact of altering Poisson's ratio and pore size of cellular scaffolds on the properties of cells growing on it. However, this approach limits its applications to in-vitro environments. The ability to remotely actuate scaffolds would allow for precise, non-invasive, and controlled activation of these engineered structures. Towards this, the current research work aimed at the design and fabrication of a dynamic metamaterial-based unit cell microstructure capable of exhibiting a varying Poisson's ratio in response to thermal stimulus. The microstructure was fabricated using a biocompatible Poly(N-isopropylacrylamide) (pNIPAM) based photoresist and a two-photon polymerization (2PP)-based direct laser writing technique. Systematic characterizations were first performed on a simplified model to evaluate the correlation between the printing parameters which include laser power, scanning speed, and hatching angles to the shape-morphing characteristics of the printed microstructures. The learnings were implemented to fabricate the proposed varying Poisson's ratio model. The fabricated microstructure exhibited a rapid and reversible change in Poisson's ratio when subjected to a thermal stimulus by virtue of the inherent properties of hydrogels and heterogeneity introduced within the structures by varying the laser parameters during the printing process. In a broader context, this research serves as the first step towards the realization of a dynamic stimulus-responsive 3D scaffold for cell culture applications.**

***Keywords*—4D Printing, Mechanical Metamaterials, Two-Photon Polymerization, Poisson's Ratio, Thermal Stimulus**

## I. Introduction

Shape morphing is a prevalent feature in all living organisms as it enables them adapt and respond to changes in their external environment [1], [2]. Incorporation of such shape-morphing capabilities into engineered structures can be of great benefit as it can result in the development of structures that are more efficient, flexible, and adaptable.

In recent years, extensive research has been conducted to develop material systems capable of exhibiting shape-morphing behavior when subjected to external stimuli. Examples of these materials include shape-memory polymers, hydrogels, dielectric elastomers, shape-memory alloys, and liquid crystalline elastomers, and are commonly referred to as smart materials. In order to fabricate complex geometries capable of exhibiting shape-morphing behavior, researchers have found ways of combining smart materials with 3D printing technology, thus allowing for direct printing of smart structures. This led to the advent of 4D printing, where 'time' constitutes the fourth dimension [3]. 4D printing is commonly defined as a fabrication technique that involves the change in shape, form, functionality, and property of a 3D printed structure over time when it is exposed to an external stimulus such as temperature, light, moisture, magnetic fields, and electric fields [4], [5], [6]. The addition of time as the fourth dimension in 4D printing allows for the creation of objects that can be pre-programmed to change their shape in response to external stimuli. The ability to print dynamic shape morphing structures has had an enormous impact on the industry in general [7], [8], and biomedical sector in particular. The development of customizable and dynamic stents [9], splints, and structures for the controlled release of drugs [10] are some examples of the application of 4D printing in the biomedical sector.

Recent developments in precision systems and software have made it possible to fabricate microstructures with excellent precision and accuracy [11], [12]. One microfabrication technique that has found widespread application in this regard is direct laser writing, based on two-photon polymerization (2PP) [13], [14]. Unlike conventional light-based photo-polymerization techniques that involve the absorption of a single photon to initiate photo-polymerization, 2PP necessitates the simultaneous absorption of two photons in a photosensitive material called the photoresist to initiate the polymerization reaction, thus resulting in extremely high accuracy of printing [14], [15]. This facilitates precise control over local polymerization, thereby enabling the incorporation of heterogeneity within a single 3D-printed microstructure by varying the local laser dosage. Consequently, varying degrees of polymerization occurs within the photoresist, giving rise to microstructures in which different sections exhibit distinct physical and mechanical properties, thereby effectively creating two distinct materials using the same photoresist solution. When these microstructures are subjected to external stimuli, the anisotropic sections exhibit contrasting levels of response, leading to complex shape-morphing behavior. A class of stimuli-responsive materials (photoresist) that have found widespread application in this regard are Poly(N-isopropylacrylamide) (pNIPAM) based hydrogels [16]. pNIPAM-based hydrogels exhibit a hydrophilic behavior at room temperature owing to the hydrogen bonds formed between the polymer chains and water molecules. This

allows pNIPAM-based hydrogels to absorb large amounts of water. However, if the temperature is increased beyond the lower critical solution temperature (LCST) of NIPAM, the polymer chains undergo a rapid transition from a hydrophilic to a hydrophobic state, resulting in the expulsion of water molecules from the hydrogel matrix. As a result, the hydrogel undergoes large volume change, thereby shrinking dramatically. The transition from a hydrophilic to a hydrophobic state is completely reversible, and the polymer chains return to their original configuration once the thermal stimulus is removed [17]. Since the LCST of pNIPAM is very close to the human body temperature and owing to its good biocompatibility, pNIPAM-based structures are well-suited for biomedical applications [18]. Additionally, the properties of pNIPAM-based hydrogels can be tuned easily, thereby enabling the hydrogel to be responsive to multiple stimuli, and at the same time exhibit large deformations when compared to other hydrogels [19], [20], [21]. Thus, combining 2PP with pNIPAM-based photoresists allows for the development of dynamic microenvironments that can interact more naturally with cellular systems, thereby closely mimicking real-life scenarios (in the domain of cell culture and tissue engineering).

One particular area that has drawn interest from researchers is to evalaute the influence of Poisson's ratio of cellular scaffolds on cell proliferation and growth [22]. In this regard, cellular scaffolds made of a class of architectured materials called mechanical metamaterials have been widely used [23], [24], [25]. Mechanical metamaterials are typically defined as engineered materials that exhibit mechanical properties which are usually not found in nature, such as negative Poisson's ratio [26], [27], [28], negative coefficient of thermal expansion [29], and negative stiffness [30]. The unusual properties exhibited by mechanical metamaterials arise due to the geometry and structure of the sub-units that make up their lattice structure rather than by the chemical composition and physical characteristics of its constituents [31]. Along with Poisson's ratio, the influence of changing pore size of scaffolds on the proliferation and growth of cells seeded within them has also emerged as a topic of interest within the scientific community [32], [33]. In order to actuate these cellular scaffolds, external cyclic mechanical loads are generally used [34], [35], [36]. However, mechanically loading these scaffolds limits their use only to laboratory conditions. The ability to remotely actuate scaffolds using stimuli such as temperature, magnetic fields, and electric fields would be highly beneficial as it would allow for precise, non-invasive, and controlled activation of the scaffolds without the need for direct contact. Additionally, the external stimuli could be applied locally or selectively, thereby allowing targeted actuation of certain regions in the scaffolds. The stimulus can also be modulated and adjusted over time, thereby allowing for dynamic control of the scaffold behaviour. In many cases, this would help in better mimicking natural physiological processes. Lastly, having scaffolds that respond to remote external stimuli enables multiple scaffolds to be simultaneously activated using a centralized or distributed stimulus source.

Towards this, the current research work aimed at the design and fabrication of a dynamic unit cell microstructure capable of reversibly changing its Poisson's ratio when exposed to an external thermal stimulus. The structure was fabricated using a 2PP-based direct laser writing technique and using a single hydrogel-based photoresist comprising of Poly(N-isopropylacrylamide) (pNIPAM). Prior to fabricating the proposed varying Poisson's ratio structure, a simplified model was first fabricated to evaluate the influence of printing parameters and geometry on the shape-morphing behavior of the microstructures when subjected to a thermal stimulus. The effect of printing parameters such as laser power, scanning speed, and hatching angles on the shape-morphing capabilities of the printed structures was investigated using the simplified model. Additionally, the influence of geometry on the shape-morphing capabilities of the microstructures was also evaluated. Understanding these properties was crucial for modeling and fabricating the proposed model capable of exhibiting a pre-programmed controlled reversible change in its Poisson's ratio.

## II. Materials and Methods

### A. Photoresist Composition and Preparation

***Photoresist Composition:*** Here, N-isopropylacrylamide (>97%) was the choice of monomer and N,N-methylenebis (acrylamide) (>99%) was the choice of cross-linker. Lithium phenyl(2,4,6-trimethylbenzoyl) phosphinate was used as a photoinitiator, and all components were dissolved in Ethylene Glycol (>99%), which served as a solvent.

***Photoresist Preparation:*** 400 mg of NIPAM was added to 450 µL of Ethylene Glycol (EG) and magnetically stirred for 3 hours. After complete dissolution, 40 mg of the cross-linker N,N-methylenebis(acrylamide) (Mbis) and 15 mg of the photo-initiator lithium phenyl(2,4,6-trimethylbenzoyl)phosphinate (LAP) were added under yellow light conditions and stirred again for 3 hours. Following this, the brown bottle containing the photoresist solution was wrapped in aluminum foil to avoid unnecessary exposure to light. An illustration of the relative proportions of each of these constituents [37] and a step-by-step preparation procedure is provided in **Appendix sectionVI-D**.

### B. Fabrication and Optical Characterization

All structures in this research were fabricated using a commercial Direct Laser Writing setup (Photonic Professional GT, Nanoscribe GmbH). An overview of the setup is provided in **Appendix section VI-E**. Prior to printing the microstructures, a 30 mm diameter glass substrate of thickness 170 µm from Thermo Scientific Inc. was first cleaned using isopropanol and acetone. This was followed

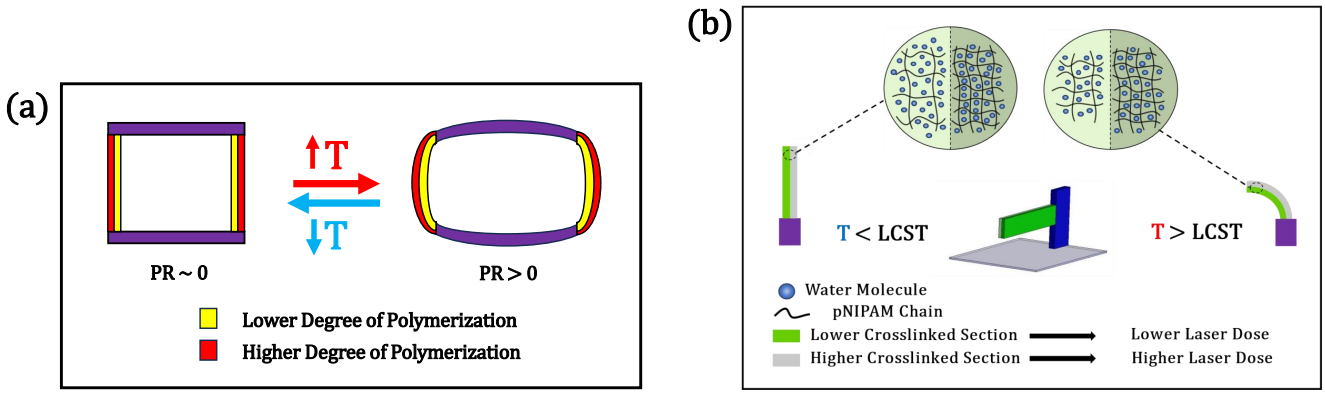


Fig. 1: **(a)**. Schematic representation of the proposed varying Poisson's ratio (PR) structure. **(b)**. Illustration of the directional deflection of beam elements due to inhomogeneous shrinkage between the two layers when subjected to a thermal stimulus

by oxygen plasma treatment of the glass substrate for 15 minutes. The treated glass substrate was then placed in a Petri dish containing a thin layer of 3-(Trimethoxysilyl)propyl Methacrylate (Stabilized with BHT, >98.0%) for 1 hour. This process, commonly referred to as silanization, ensures that the microstructures printed on the glass substrate adhere firmly to it, thereby reducing the chances of delamination of the structures (**Appendix section VI-F**). Following silanization, the glass substrate was again cleaned using isopropanol and acetone. The glass substrate was then firmly mounted onto the substrate holder using tape to hold it in place. Since the oil configuration was used for fabricating the structures, a drop of immersion oil (Immersol 518F, ZEISS) was placed on the side of the substrate facing the objective.

Next, a drop of the pNIPAM-based photoresist was placed on the other side of the glass substrate, and the sample holder was loaded into the printer. A 25x oil immersion objective (numerical aperture of 0.8 from ZEISS) was used for printing the microstructures, the details of which can be found in **Appendix Table I**. Once the printing process (**Appendix section VI-G**) was completed, the excess precursor solution was rinsed away using acetone followed by rinsing using ultrapure water. Finally, the glass substrate was kept submerged in ultrapure water for 2 hours before testing (**Appendix section VI-H**). Since the microstructures are hydrogel-based, the substrate was always kept immersed in water. This was followed by optical characterization of the printed structures using an Olympus CKX 53 microscope. An overview of the setup used for characterization is provided in **Appendix section VI-I**.

### *C. Design Methodology*

An illustration of the design of the proposed changing Poisson's ratio model is as shown in **Figure.1.(a)**. The proposed model consists of a virtual bi-layered design (in two segments of the model) introduced in the structure by varying the laser exposure within the photoresist during the fabrication process. Varying the laser exposure results in different degrees of cross-linking within the structure printed (**Appendix section VI-B**). At room temperature, the structure, by virtue of its design and geometry, is expected to exhibit a near-zero Poisson's ratio (PR). However, when subjected to a thermal stimulus (i.e. above LCST of NIPAM), the amount of water expelled from the differently cross-linked sections is not the same, thereby causing the structure to morph in a certain predetermined manner. The morphed structure, by virtue of its geometry, is expected to show a large positive Poisson's ratio. Since reversibility is a key factor for this research work, the proposed structure is expected to return to its original configuration upon reducing the temperature below the LCST of NIPAM.

In order to fabricate the proposed structure, multiple factors had to be determined. Suitable printing parameters, namely the laser power, scanning speed, hatching angles, hatching, and slicing distance that allow for the desired shape-morphing behavior to occur had to be determined. Additionally, a suitable geometric design and printing strategy that would facilitate the desired shape-morphing behavior had to be devised. Additionally, for the bi-layered elements of the model, an optimum combination of laser dosage (laser power, scanning speed) that allows for the desired deformation to occur had to be found. Since evaluating these parameters directly in the final proposed model would involve large printing times and increased complexity, a simple bi-layered microcantilever beam as shown in **Figure.1.(b)** was first fabricated and the above-mentioned characterizations were performed on it. The bi-layer effect in the cantilever beam was introduced by varying the printing parameters (i.e laser power and scanning speed) within the same structure as discussed earlier. This results in one section of the beam to have a lower cross-linking density than the other. Upon exposure to an external temperature stimulus, the two layers exhibit different amounts of shrinkage, thereby resulting in a

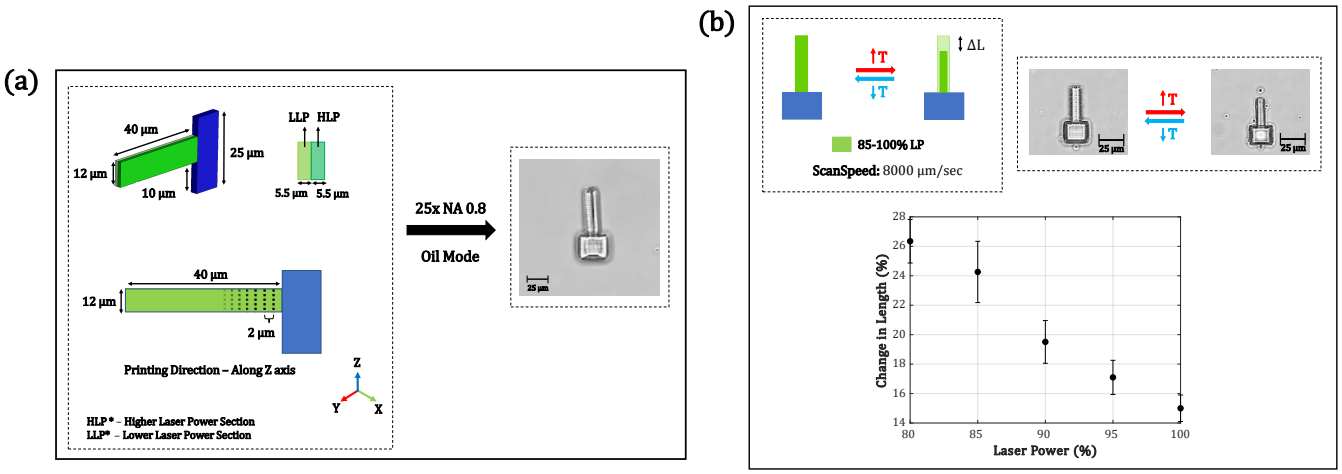


Fig. 2: **(a)**. Illustration of the printing strategy adopted to fabricate the proposed bi-layered cantilever beam. The figure on the left depicts the overall dimensions of the beam and the printing strategy adopted. The beam fabricated using 2PP is shown in the image on the right (Scale: 25 µm). **(b)**. Characterizing the effect of laser power on lateral shrinkage of the beam

directional deformation of the beam. An illustration of this concept is as shown in the **Figure.1.(b)**.

The term laser dose in **Figure.1.(b)** corresponds to the amount of energy delivered by the laser to the photoresist and is a function of the laser power and laser scanning speed. A higher laser dose corresponds to a higher degree of polymerization as compared to a section printed using a reduced laser dosage. It is to be noted that a higher degree of polymerization can be achieved either by increasing the laser power at a given scanning speed, or reducing the scanning speed at a fixed laser power, or simultaneously increasing the laser power and reducing the scanning speed. The methods adopted to change the laser dosage in order to maximize the deformation in the proposed bi-layered beam structure will be discussed in detail in the 'Results and Discussions' section. A mathematical overview of the directional deformation of a bi-layered beam element is provided in **Appendix section VI-C**.

## III. Results and Discussions

### A. *Dose Test*

To determine the appropriate combinations of the laser power and scanning speed that are capable of inducing sufficient polymerization in the pNIPAM-based photoresist, a dose test was performed. A matrix of multiple cuboidal samples each of dimensions 20 µm x 20 µm x 15 µm was fabricated by varying the laser power (60% to 100% of the maximum power (50mW) in increments of 4%) and scanning speed ( 1,500 µm/sec to 11,500 µm/sec in steps of 1,000 µm/sec) as depicted in **Appendix (section VI-J, Figure 21**). The results of the dose test (**Appendix section VI-J, Figure 22**) revealed that for the given recipe of pNIPAM photoresist, laser power and scanning speeds in the range of 75 - 100% (of maximum laser power) and 6,000 µm/sec – 11,500 µm/sec respectively produced structures that exhibit an acceptable amount of polymerization. Following optical characterization of the cuboidal microstructures, a suitable choice of laser power and scanning speed was made to print the bi-layered cantilever beam model.

### B. *Printing and Characterization of Bi-layered Beam Model*

***Optimized Printing Strategy:*** A dimensional overview of the bi-layered beam fabricated is as shown in **Figure.2.(a)**. It is to be noted here that the conventional direction of printing in DeScribe (software for print job development from Nanoscribe) is along the X-Y plane, i.e., individual layers are printed along the X-Y plane, and the layers are stacked up on each other along the Z-axis to obtain the desired structure. However, due to the low scanning speed used for printing the microstructures (8,000 µm/sec), delamination was observed between two consecutive layers along the Z-axis. Therefore, the printing strategy was changed such that small sections (of 2 µm length) were printed in the X-Z plane and extended along the Y-axis (length of beam). An overlap of 0.75 µm was provided between the higher and lower polymerized sections of the beam to prevent delamination in the structure when subjected to thermal loads. Additionally, between the beam element and the fixed post, an overlap of 2 µm was provided to ensure structural stability of the overhanging structure. A detailed description of the characterizations performed to find the optimum values of overlap mentioned above is provided in **Appendix section VI-L**.

Following fabrication, some microstructures were present in an unintended deformed state. It is hypothesized that residual stresses present in the structure is the underlying cause for this behavior. To relieve the structures of residual stresses and return the structures back to their original intended configuration, a stress-relieving annealing process was adopted, the details of which can be found in **Appendix**

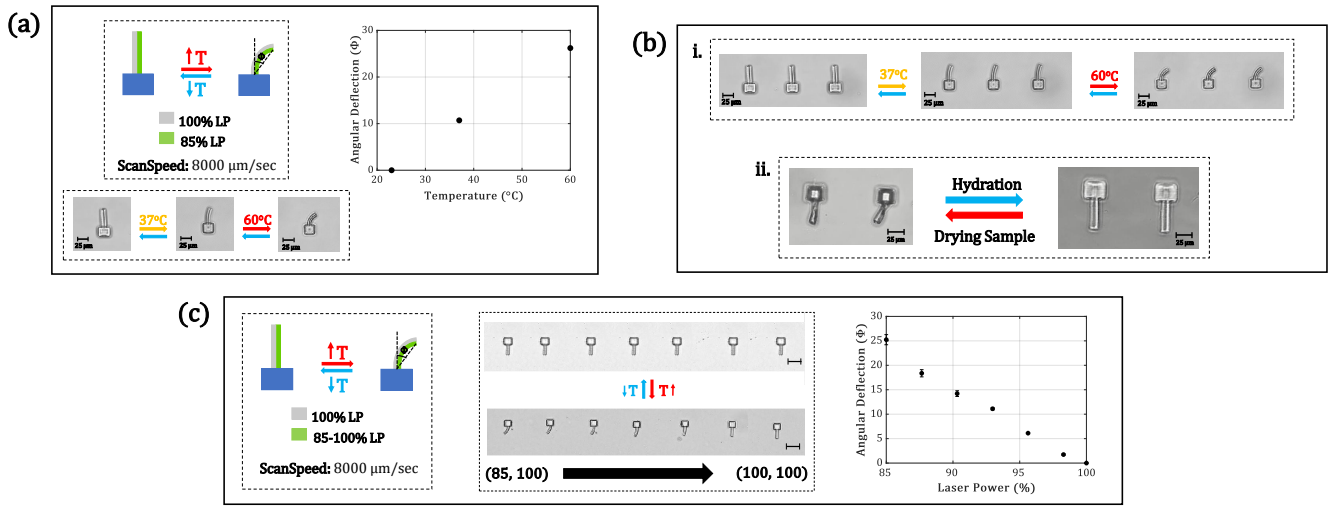


Fig. 3: **(a)**. Characterizing the effect of temperature on the angular deflection of the beam (Scale: 25 µm). **(b)**. (i). Evaluating the repeatability of angular deformation of beams when subjected to different thermal loads (Scale: 25 µm). (ii). Evaluating the impact of drying and rehydrating the beam on its geometry and shape-morphing ability (Scale: 25 µm). **(c)**. Evaluating the effect of different laser power combinations on the angular deflection of beams (Scale: 50 µm)

**section VI-K**.

***Characterization of Bi-Layer Beam Model:*** The bi-layered microcantilever beams were subjected to thermal loads following fabrication, and their shape-morphing behavior was characterized as a function of printing parameters, thermal stimulus, and geometry of the microstructure.

***Effect of Laser Power on Shrinkage:***
Since shrinkage of the beam elements upon being subjected to a thermal stimulus is the underlying cause for the directional deflection of the beams, it was essential to examine the influence of laser dosage on the degree of shrinkage exhibited by these structures. To evaluate this, the laser power used to print the beam section of the model was varied from 85% to 100% in increments of 5%, and the relative change in length of the beam elements was recorded when the structures were subjected to a thermal stimulus of 60°C. For the given characterization, a constant scanning speed of 8000 µm/sec was used to print the structures, and a slicing and hatching distance of 0.3 µm and 0.2 µm respectively was used. It is to be noted here that all structures printed as part of this research consist of slicing and hatching distances as mentioned above. The results obtained are presented in **Figure.2.(b)**.

From the plot in **Figure.2.(b)**, it is evident that the beam sections printed with a comparatively lower laser power show a larger extent of shrinkage. This can be attributed to the extent of polymerization and in turn the extent of cross-linking induced within the structure when exposed to varying degrees of laser power. The set of samples used to characterize the extent of shrinkage of beam elements for different laser powers is as shown in **Appendix section VI-M**. Additional characterizations were performed to evaluate the influence of laser power on the coefficient of thermal expansion of the beam elements, the details of which can be found in **Appendix section VI-N**. Utilizing this difference in shrinkage, dynamic shape-morphing behavior can be achieved by combining two such elements and subjecting them to the same thermal load, as illustrated in the characterizations provided below.

***Impact of Temperature on Beam Deformation:***
Utilizing the difference in the extent of shrinkage in beam elements when printed using different laser doses, bi-layered cantilever beams were fabricated using a combination of different laser powers as illustrated in **Figure.3.(a)**. Next, the beams were subjected to two different thermal loads, one at 37°C and the other at 60°C, and their angular deflections were evaluated as a means of characterizing the extent of shape-morphing behavior these structures exhibit as a function of thermal loads. The response of the beam when subjected to a temperature of 37°C indicates that the microcantilever structure is capable of exhibiting a dynamic and reversible response at human body temperature. The beams were further subjected to a higher thermal load (60°C) and their response was recorded. It is evident from the plot in **Figure.3.(a)** that the angular deformation of the beam increases with an increase in temperature. Additionally, the angular deformation is completely reversible and the beam returns to its original configuration once the temperature is bought back to 23°C (room temperature).

In order for the design to be reliable, the shape-morphing behavior must be repeatable over multiple cycles, and the design must be inherently robust. To ensure this, the fabricated

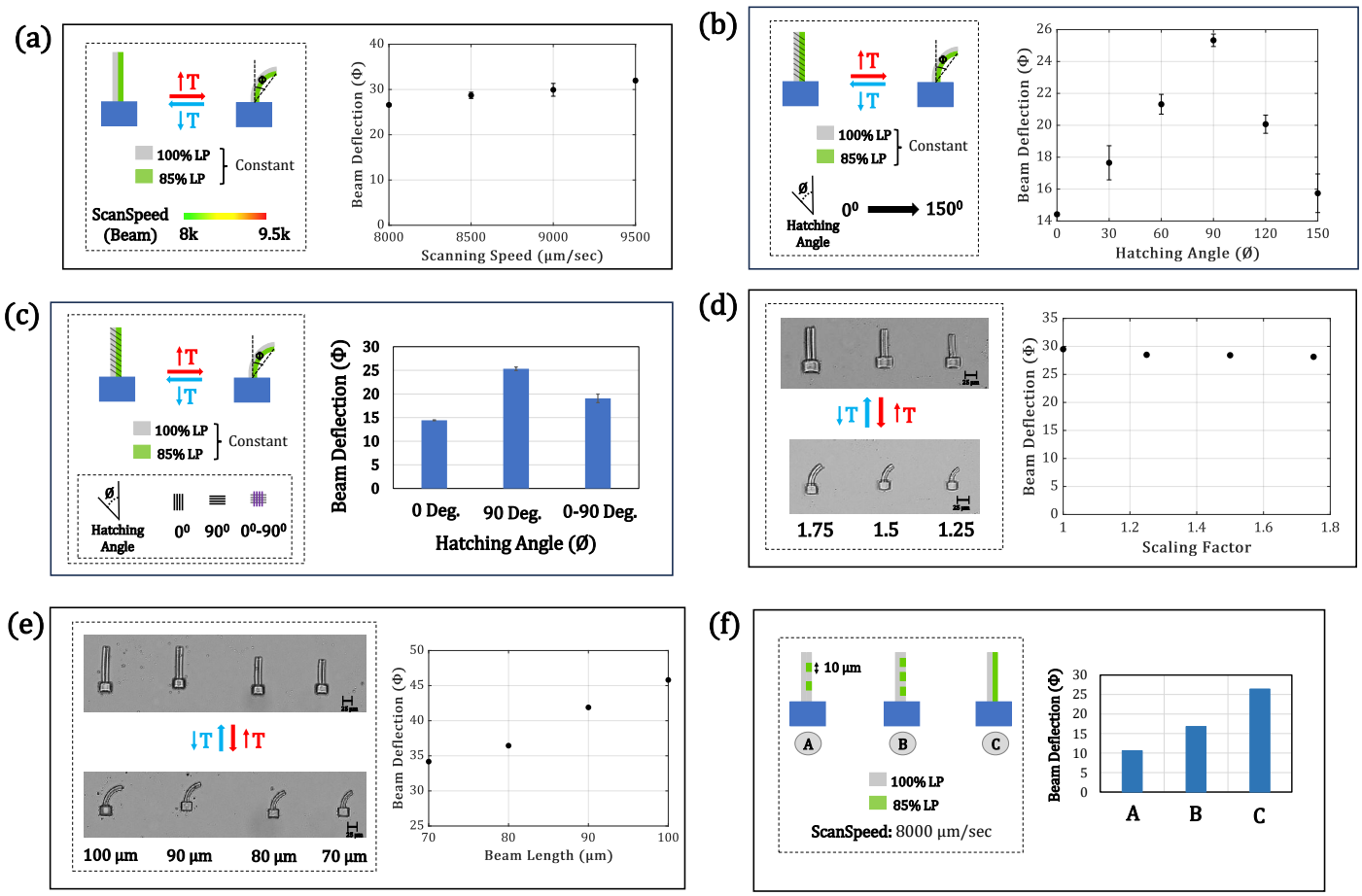


Fig. 4: **(a)**.Evaluating the effect of laser scanning speed on the angular deflection of beams. **(b)**. Evaluating the effect of hatching angle on the angular deflection of beams. **(c)**. Evaluating the influence of hatching lines orientation on the angular deflection of beams. **(d)**. Evaluating the effect of scaling on the angular deflection of beams (Scale: 25 µm). **(e)**. Evaluating the effect of beam length on the angular deflection of beams (Scale: 25 µm). **(f)**. Evaluating the effect of the distribution of lower polymerized sections on the angular deflection of beams

models were subjected to multiple cycles of thermal loads as shown in **Figure.3.(b).i**, and their deformations were recorded. In each cycle, nearly identical and reversible shape-morphing behavior was observed, thus ensuring the repeatability of the desired deformation. Additionally, a test was performed where the beams were dried and then hydrated back again as shown in **Figure.3.(b).ii** to understand the influence of drying on the structural integrity of the structure. It was observed that the beams returned to their original shape and size once hydrated, thereby confirming the robustness of the printed structure.

***Impact of Different Laser Power Combinations on Beam Deformation:***

To understand the influence of different laser power combinations on the angular deflection of the beam when subjected to thermal loads, a characterization was performed where the laser power of one section of the beam was kept constant (100% of maximum laser power) while the laser power of the other section was increased from 85% to 100% in steps of approximately 3%, as illustrated in **Figure.3.(c)**. The results obtained (plot in **Figure.3.(c)**) clearly indicate that a greater difference in laser power between the two layers corresponds to a greater angular deflection of the beams when subjected to a thermal load of 60°C. Amongst the combination of laser powers selected to fabricate the beam, a difference in laser power of 15% between the two segments of the bi-layered beam (with one segment fixed at 100% laser power) yielded the largest angular deflection of about 25 degrees. Additionally, a near linear (and inversely proportional) relation between the angular deflection and laser power combinations was observed when the laser power chosen to fabricate the lower polymerized section was gradually increased to 100% of the maximum laser power. This is consistent with the theory of difference in the cross-linking densities as explained in **Appendix section VI-B**. Additionally, when both layers of the beam were printed using 100% laser power, the beam did not show

any angular deflection. This confirms that the difference in laser dosage between the two segments of the beam is the underlying reason for its shape-morphing behavior. The array of microcantilever beams used to evaluate the mean and standard deviations for different cases can be found in **Appendix section VI-O**.

***Impact of Scanning Speed on Beam Deformation:***
To characterize the influence of scanning speed on the shape-morphing capabilities of the structure, the bi-layered section of the beam was printed using scanning speeds ranging from 8000 µm/sec to 11,000 µm/sec in increments of 500 µm/sec, and evaluated for its angular deflection when exposed to a thermal stimulus of 60°C. The results obtained are as shown in **Figure.4.(a)**.

It is to be noted here that the combination of laser powers is kept constant in each case. It is evident from the plot in **Figure.4.(a)** that an increase in the scanning speed results in a proportional increase in the angular deflection of the beam. Within the range of assessed scanning speeds for the given combination of laser powers, it was observed that a relative increase of about 18% in the scanning speed resulted in an approximately 20% increase in the relative angular deflection of the beams. While fabricating the structures, it was observed that for the given combination of laser powers, a scanning speed beyond 9,500 µm/sec was not sufficient enough to polymerize the photoresist adequately to obtain the desired bi-layered configuration. A discussion on this is provided in **Appendix section VI-P**. When viewed in terms of cross-linking densities and in turn the extent of polymerization, increasing the laser scanning speed directly translates to a reduced laser dosage, thus resulting in a lower degree of cross-linking in the structure. This gives rise to a greater extent of deformation (up to a certain threshold beyond which insufficient polymerization occurs) when subjected to a thermal stimulus. Since the laser scanning speed and the cross-linking density are inversely proportional to each other, a trade-off has to be made between structural stability and shape-morphing capability when it comes to 4D printing of dynamic microstructures. A conclusion that can be drawn from the results obtained from characterizing the influence of laser power and scanning speeds (plots in **Figure.3.(c)** and **Figure.4.(a)**) is that for the given set of printing and geometric parameters, greater deflection can be achieved by varying the laser power combinations as compared to increasing the scanning speeds used to print the beam elements.

***Impact of Hatching Angle on Beam Deformation:***
The influence of hatching angle on the angular deflection of beams was evaluated by printing various beams with hatching angles ranging from 0° to 150°. A brief overview of the concept of hatching is provided in **Appendix section VI-Q**. The beams were subjected to a thermal stimulus of 60°C and the corresponding angular deformations were recorded (**Figure.4.(b)**).

The results obtained clearly indicate that for a given combination of laser powers and scanning speed, the hatching angle plays an important role in determining the extent of beam deformation. Here, increasing the hatching angle from 0° to 90° resulted in about a 75% relative increase in the angular deflection of the beam segment. The angular deflection of the beam increased steadily till a hatching angle of 90°. Beyond this point, an increase in the hatching angle resulted in a steady decline in the beam deflection. It is to be noted here that both the higher and lower polymerized sections of the beam share the same hatching angle. A study was also conducted to evaluate the effect of printing the beam with hatching lines that change from 0° to 90° for each subsequent layer printed (**Figure.4.(c)**). It is evident from the results that having subsequent hatching lines that are oriented at 90° to one another gives an angular deflection that is larger than a beam with all hatching lines oriented at an angle of 0° (a relative increase of about 32% in angular deflection of beams). This strategy can be adopted to enhance the strength and stability of the structure, while simultaneously retaining its shape-morphing characteristics to a good extent. Additionally, anisotropy within the structure can also be reduced using this technique, which might be beneficial in some cases. Additional characterizations pertaining to hatching angles were also performed and can be found in **Appendix section VI-Q**.

***Impact of Scaling on Beam Deformation:***
In some cases, the fabricated model would need to be scaled up based on the desired application or the space constraints present in a system. Therefore, the impact of scaling the structure on its shape-morphing characteristics was evaluated. The bi-layered cantilever beam model was scaled up using the scaling factors as shown in **Figure.4.(d)**. The results from the thermal stimulus test reveal that scaling up the model had a negligible impact on the angular deflection of the beam. It's important to note here that there exists a threshold beyond which scaling can influence the shape-morphing behavior of the structure. A large value of scaling factor might result in the structure being too large to print using the oil mode, and given the overhanging nature of the design and the properties of the photoresist, the structure would likely collapse under its own weight. However, for the proposed application of this research, the structures are desired to be in the micron range thus making this study on scaling relevant to this research.

***Impact of Beam Length on Beam Deformation:***
Another characterization performed towards evaluating the impact of beam geometry on its shape-morphing capability was to determine the influence of beam length on its angular deflection. The length of the beam was increased from 70 µm to 100 µm in steps of 10 µm as shown in **Figure.4.(e)**.

All other parameters pertaining to the beam section, namely

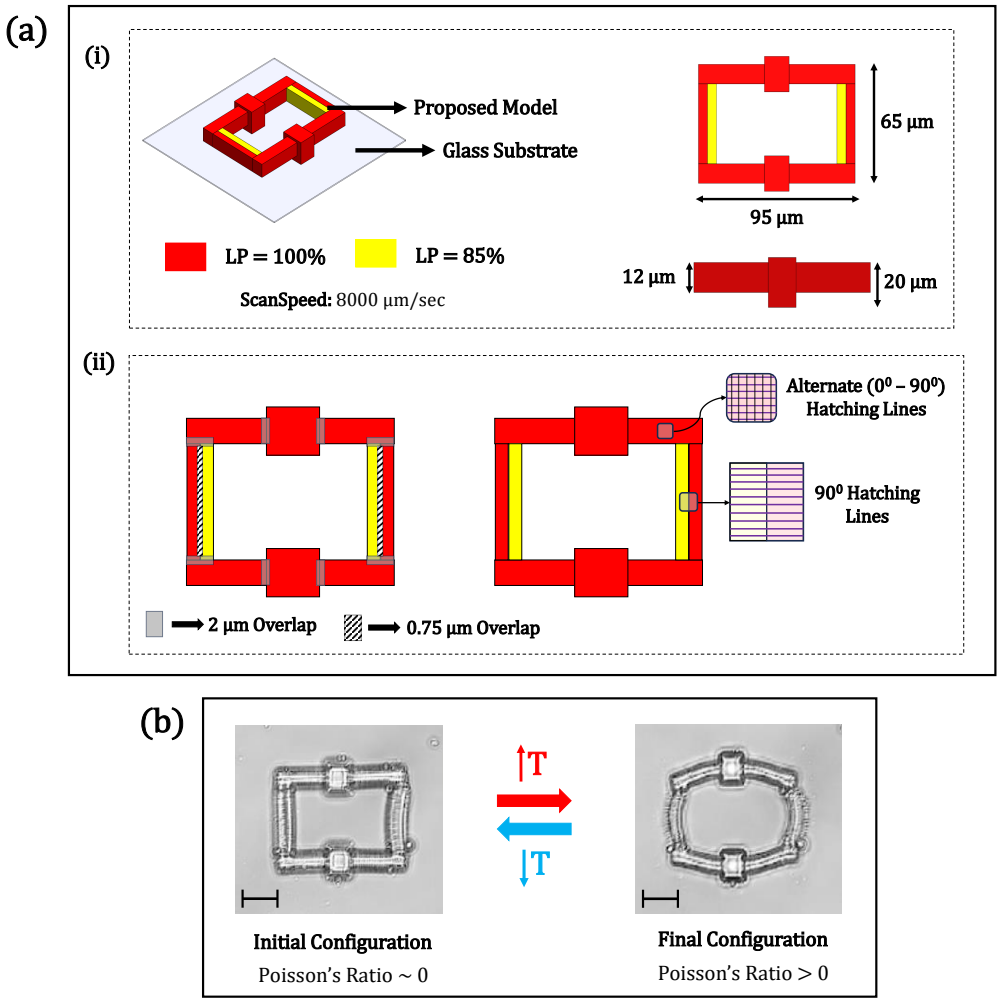


Fig. 5: Overview of varying Poisson's ratio model. **(a)**. (i). Overall dimensions of the structure along with the laser dosage used for fabrication. (ii). Illustration of the printing strategies adopted to ensure robustness of design. **(b)**. Model fabricated using 2PP and subjected to thermal stimulus. The structure undergoes a reversible and near-instantaneous change in Poisson's ratio (Scale: 30 µm)

the width (19.25 µm) and height (21 µm) were kept constant. It can be inferred from the results (plot in **Figure.4.(e)**) that increasing the length of the beam was accompanied by a corresponding increase in its angular deflection. For the given choice of printing parameters, a 30 µm increase in the length of the beam resulted in approximately a 34% increase in its relative angular deflection. Again, as with the case of scaling the structure, there is a limit beyond which the length of the overhanging beam elements cannot be extended as it would collapse under its own weight. The threshold value depends on the properties of the photoresist used to print the structures, and also the choice of printing parameters.

***Impact of Spatial Distribution of Lower Polymerized Sections on Beam Deformation:***

A characterization was performed to evaluate the impact of the distribution of lower polymerized sections within the bi-layered beam design on its angular deflection. Three beams with different distributions of the lower polymerized section (**Case A**, **Case B**, and **Case C** of **Figure.4.(f)**) were printed and their deformations were evaluated when subjected to a thermal stimulus of 60°C. From the results obtained, it is clear that in order to achieve a larger extent of deflection in the structure, it is preferable to have a continuous distribution of the lower polymerized section instead of having intermittent regions in the structure that are printed using a lower laser dose.

Moreover, a characterization was conducted to evaluate the effect of varying the thickness of each layer within the bi-layered cantilever beam on its shape-morphing behavior and is discussed in detail in **Appendix section VI-R**. Further-

more, tests were conducted to evaluate the response of the microstructures to different solvents (isopropanol and acetone) as well as their sensitivity across different pH levels. The results obtained can be found in **Appendix section VI-S** and **Appendix section VI-T** respectively.

### *C. Changing Poisson's Ratio Model*

The final proposed model exhibiting a varying Poisson's ratio was designed taking into account the information gathered from characterizing the bi-layered microcantilever beams. An illustration of the final proposed design is as shown in **Figure.5.(a)**.

The model consists of six over-hanging beam elements which are held in place by two posts attached to the glass substrate. The overhanging structures were printed using the strategy of printing small sections of 2 µm length along the Z-axis, as developed while printing the bi-layered beam (**Figure.2.(a)**). This ensured structural integrity of the overhanging elements of the model, and avoided the possibility of delamination between layers. In order to achieve the desired deformation, two sections of the beam were printed using the bi-layered configuration as discussed earlier. Each of these two layers consists of a continuous distribution of their corresponding laser dosages in order to maximize the deformation, as determined while characterizing the bi-layered cantilever model (**Figure.4.(f)**). Additionally, an overlap of 0.75 µm was provided between the higher and lower polymerized segments of the beam to prevent delamination between the layers. An overlap of 2 µm was provided between each of the six segments as depicted in **Figure5.(a).ii** to prevent delamination between different elements when subjected to a thermal stimulus.

Based on the results obtained from characterizing the microcantilever beams, optimum printing parameters were chosen to fabricate the final proposed structure. The two sections consisting of the bi-layered design were printed using a laser power combination of 100% and 85% of the maximum laser power (50 mW). All other structures in the model were fabricated using 100% of the maximum laser power. A constant laser scanning speed of 8000 µm/sec was employed to print the model. Given the nature and objective of the proposed design, it was necessary to ensure that the sections of the model consisting of a bi-layered design exhibited maximum deformation when subjected to a thermal stimulus, while the other four overhanging structures supporting these bi-layered sections provided optimum structural support while simultaneously remaining compliant enough to allow for the desired deformation. Drawing inspiration from the results depicted in **Figure.4.(b)** and **Figure.4.(c)**, the bi-layered segments of the structure were printed using a hatching angle of 90°, while the four overhanging structures were printed with alternate hatching angles of 0° and 90° as depicted in **Figure.5.(a).ii**. Additionally, the configuration of alternating hatching lines represents a woodpile structure, thus ensuring good structural integrity while simultaneously allowing for the desired deformation.

The final fabricated model is shown in **Figure.5.(b)** . The structure, by virtue of its geometry [38], exhibited a near-zero Poisson's ratio at room temperature. Upon subjecting the microstructure to a thermal stimulus of 60°C, a rapid and near instantaneous shape change (response time of approximately 1 second) was observed and the structure transformed into a geometry (closely resembling the honeycomb structure) that displays a large positive value of Poisson's ratio. It is to be noted here that this shape change was completely reversible and the structure returned to its original configuration once the thermal stimulus was removed. In order to evaluate the robustness of the design and the repeatability of the desired shape-morphing behavior, the microstructure was subjected to multiple thermal cycles, and the deformation of the structure was evaluated in each case. The deformation was observed to be repeatable and there was negligible difference in the shape-morphing behavior of the structure over multiple cycles. Thus, a microstructure capable of exhibiting a varying Poisson's ratio when subjected to a thermal stimulus was successfully fabricated and tested, thereby achieving the aim of this research work.

## IV. Conclusions

In conclusion, a comprehensive design and fabrication strategy aimed at fabricating a microstructure capable of exhibiting a reversible change in its Poisson's ratio was developed. A single material and single-step fabrication process based on 2PP direct laser writing and pNIPAM-based hydrogels was used to fabricate microstructures capable of exhibiting a reversible and near instantaneous change in their geometry upon being subjected to an external thermal stimulus. Shape-morphing capability was induced by introducing anisotropy within the fabricated microstructures by locally varying the printing parameters (laser power, scanning speed, and hatching angles). Systematic characterizations were first performed on a simplified bi-layered cantilever beam model to evaluate the influence of printing parameters and geometry on the shape-morphing characteristics of the microstructures. The learnings were then implemented to model and fabricate the changing Poisson's ratio model. The final fabricated model, when subjected to a thermal stimulus, underwent a rapid and reversible transformation from a geometry characterized by a near-zero Poisson's ratio to a geometry that exhibits a large positive value of Poisson's ratio, thus achieving the aim of this research. In a broader context, this research serves as the first step towards the realization of a dynamic 3D scaffold that can swiftly respond to external stimuli. Furthermore, the results obtained in this research reaffirm the vast potential of pNIPAM-based hydrogel microstructures within the realm of biomedicine, opening up new frontiers for further exploration and innovation.

## V. Limitations and Future Work

While the current research successfully achieved its goal of fabricating a structure capable of exhibiting a varying Poisson's ratio, and is a stride made in the direction of developing stimulus-responsive hydrogel-based scaffolds for tissue engineering applications, there remain a few limitations and opportunities for future improvement. Some of these areas include:

- ***Mechanical characterization:*** To gain deeper insights on the influence of printing parameters on the properties of the structures, conducting thorough mechanical characterization is essential. Nanoindentation testes need to be performed on the samples fabricated as part of the dose test in order to assess properties such as stiffness of the structures. The characterization should also be performed on the microstructures when a temperature stimulus is provided to it. It is well known that the mechanical properties of pNIPAM-based structures change when subjected to a temperature greater than LCST. This characterization will provide a quantitative measure of the change in properties for the photoresist in use.
- ***Achieving considerable deformations at human body temperature:*** In all the characterizations performed, the microstructures were subjected to a temperature stimulus of 60°C. However, this temperature is not suitable for cell culture as it would damage the cells growing on the scaffold. Thus, suitable changes need to be made in the photoresist preparation protocol (such as reducing the LCST of NIPAM), geometric design, and printing strategies in order to achieve shape-morphing behavior at around 37°C. Some of the techniques that can be used for changing the properties of pNIPAM-based hydrogels can be found in literature [39], [40], [41].
- ***Excessive shrinkage in structures:*** pNIPAM-based structures exhibit excessive shrinkage when subjected to a thermal stimulus. Though this is advantageous in obtaining the desired shape-morphing behaviour, it can be a possible limitation if structures with good dimensional accuracy are required.
- ***Crystallization of photoresist:*** The photoresist prepared for this research was extremely sensitive to temperature change. The photoresist solution underwent crystallization when exposed to a temperature below 19°C and would return back to the liquid state at 20°C. This necessitated prolonged stirring of the photoresist solution prior to printing.
- ***Inducing temperature change using controlled thermal bath:*** During experimentation, temperature change was bought about instantaneously in the environment surrounding the microstructures. However, a better understanding of the temperature-induced deformations can be achieved by implementing controlled, incremental temperature changes using a temperature-controlled thermal bath.
- ***Combining multiple unit cells to form a lattice structure:*** Expanding upon the current unit cell lattice structure characterization, a complete lattice capable of exhibiting a varying Poisson's ratio in response to thermal stimuli should be developed.
- ***Cell-seeding on scaffold:*** Since the scaffolds are intended for cell culture applications, cell seeding needs to be performed on these scaffolds in order to assess both the structure's biocompatibility and its ability to undergo the desired reversible shape change when cells are introduced.
- ***Fabricating 3D scaffolds:*** The final step towards realizing a thermo-responsive hydrogel-based metamaterial scaffold is to fabricate a 3D scaffold capable of exhibiting a varying Poisson's ratio. A few challenges can be encountered at this step due to the weak mechanical properties of pNIPAM-based structures [18], which make the stacking of multiple unit cells on top of each other a challenging task. Additionally, since the structures are printed using the oil mode, shading will become a matter of concern during the fabrication process. The maximum height of structures that can be printed using the oil mode is limited, thus adding additional complexity to the fabrication procedure.
- ***Magnetic stimulus for inducing deformation:*** Though providing thermal stimulus to induce actuation of scaffolds is far better than actuating structures using external mechanical loads, continuously subjecting cells to changing temperatures might have a detrimental impact on cells. Thus, a stimulus which can induce shape change without affecting the cells would be ideal. One possible way to achieve this is by introducing magnetic particles to the photoresist solution, thereby creating magnetic responsive structures. Due to the complexity involved in preparing photoresists containing magnetic particles [42], this approach was not adopted for the thesis. However, the fabrication of magnetic responsive hydrogel-based micro-scaffolds would be an interesting topic for future research.

All characterizations performed as part of this thesis were experimental-based. Developing analytical models for these structures and carrying out simulations in parallel to the experimental study would be beneficial to better understand, compare and validate the results obtained. Therefore, though this research work served as the first step towards the fabrication of a dynamic stimulus-responsive hydrogel-based metamaterial scaffold, there is still a great deal of work to be done before a robust 3D stimulus-responsive lattice structure can be realized and employed for cell culture applications.

## REFERENCES


1 Oliver, K., Seddon, A., and Trask, R. S., "Morphing in nature and beyond: a review of natural and synthetic shape-changing materials and mechanisms," pp. 10 663–10 689, 12 2016.

2 Erb, R. M., Sander, J. S., Grisch, R., and Studart, A. R., "Self-shaping composites with programmable bioinspired microstructures," *Nature Communications*, vol. 4, 2013.

3 Zhang, Z., Demir, K. G., and Gu, G. X., "Developments in 4D-printing: a review on current smart materials, technologies, and applications," *International Journal of Smart and Nano Materials*, vol. 10, no. 3, pp. 205–224, 7 2019.

4 Ahmed, A., Arya, S., Gupta, V., Furukawa, H., and Khosla, A., "4D printing: Fundamentals, materials, applications and challenges," 7 2021.

5 Mitchell, A., Lafont, U., Hołyńska, M., and Semprimoschnig, C., "Additive manufacturing — A review of 4D printing and future applications," pp. 606–626, 12 2018.

6 Fu, P., Li, H., Gong, J., Fan, Z., Smith, A. T., Shen, K., Khalfalla, T. O., Huang, H., Qian, X., McCutcheon, J. R., and Sun, L., "4D printing of polymers: Techniques, materials, and prospects," 3 2022.

7 Ntouanoglou, K., Stavropoulos, P., and Mourtzis, D., "4D printing prospects for the aerospace industry: A critical review," in *Procedia Manufacturing*, vol. 18. Elsevier B.V., 2018, pp. 120–129.

8 López-Valdeolivas, M., Liu, D., Broer, D. J., and Sánchez-Somolinos, C., "4D Printed Actuators with Soft-Robotic Functions," *Macromolecular Rapid Communications*, vol. 39, no. 5, 3 2018.

9 Ge, Q., Sakhaei, A. H., Lee, H., Dunn, C. K., Fang, N. X., and Dunn, M. L., "Multimaterial 4D Printing with Tailorable Shape Memory Polymers," *Scientific Reports*, vol. 6, 8 2016.

10 Malachowski, K., Breger, J., Kwag, H. R., Wang, M. O., Fisher, J. P., Selaru, F. M., and Gracias, D. H., "Stimuli-responsive theragrippers for chemomechanical controlled release," *Angewandte Chemie - International Edition*, vol. 53, no. 31, pp. 8045–8049, 7 2014.

11 Sun, H. C. M., Liao, P., Wei, T., Zhang, L., and Sun, D., "Magnetically powered biodegradable microswimmers," *Micromachines*, vol. 11, no. 4, 4 2020.

12 Park, J., Jin, C., Lee, S., Kim, J. Y., and Choi, H., "Magnetically Actuated Degradable Microrobots for Actively Controlled Drug Release and Hyperthermia Therapy," *Advanced Healthcare Materials*, vol. 8, no. 16, 8 2019.

13 Xing, J. F., Zheng, M. L., and Duan, X. M., "Two-photon polymerization microfabrication of hydrogels: an advanced 3D printing technology for tissue engineering and drug delivery," *Chemical Society Reviews*, vol. 44, no. 15, pp. 5031–5039, 8 2015.

14 Koo, S., "Advanced micro-actuator/robot fabrication using ultrafast laser direct writing and its remote control," pp. 1–21, 12 2020.

15 Maruo, S. and Kawata, S., "Two-photon-absorbed near-infrared photopolymerization for three-dimensional microfabrication," *Journal of Microelectromechanical Systems*, vol. 7, no. 4, pp. 411–415, 12 1998.

16 Spiegel, C. A., Hippler, M., Münchinger, A., Bastmeyer, M., Barner-Kowollik, C., Wegener, M., and Blasco, E., "4D Printing at the Microscale," *Advanced Functional Materials*, vol. 30, no. 26, 6 2020.

17 Dharmasiri, M. B. and Mudiyanselage, T. K., "Thermo-responsive poly(N-isopropyl acrylamide) hydrogel with increased response rate," *Polymer Bulletin*, vol. 78, no. 6, pp. 3183–3198, 6 2021.

18 Ansari, M. J., Rajendran, R. R., Mohanto, S., Agarwal, U., Panda, K., Dhotre, K., Manne, R., Deepak, A., Zafar, A., Yasir, M., and Pramanik, S., "Poly(N-isopropylacrylamide)-Based Hydrogels for Biomedical Applications: A Review of the State-of-the-Art," 7 2022.

19 Huang, T.-Y., Huang, H.-W., Jin, D. D., Chen, Q. Y., Huang, J. Y., Zhang, L., and Duan, H. L., "Four-dimensional micro-building blocks," Tech. Rep., 2020. [Online]. Available: https://www.science.org

20 Jia, Y., Spiegel, C. A., Welle, A., Heißler, S., Sedghamiz, E., Liu, M., Wenzel, W., Hackner, M., Spatz, J. P., Tsotsalas, M., and Blasco, E., "Covalent Adaptable Microstructures via Combining Two-Photon Laser Printing and Alkoxyamine Chemistry: Toward Living 3D Microstructures," *Advanced Functional Materials*, 2022.

21 Sydney Gladman, A., Matsumoto, E. A., Nuzzo, R. G., Mahadevan, L., and Lewis, J. A., "Biomimetic 4D printing," *Nature Materials*, vol. 15, no. 4, pp. 413–418, 4 2016.

22 Yarali, E., Zadpoor, A. A., Staufer, U., Accardo, A., and Mirzaali, M. J., "Auxeticity as a mechanobiological tool to create meta-biomaterials," *ACS Applied Bio Materials*, 7 2023.

23 Zhang, W., Soman, P., Meggs, K., Qu, X., and Chen, S., "Tuning the poisson's ratio of biomaterials for investigating cellular response," *Advanced Functional Materials*, vol. 23, no. 25, pp. 3226–3232, 7 2013.

24 Mardling, P., Alderson, A., Jordan-Mahy, N., and Maitre, C. L. L., "The use of auxetic materials in tissue engineering," pp. 2074–2083, 4 2020.

25 Soman, P., Lee, J. W., Phadke, A., Varghese, S., and Chen, S., "Spatial tuning of negative and positive Poisson's ratio in a multi-layer scaffold," *Acta Biomaterialia*, vol. 8, no. 7, pp. 2587–2594, 2012.

26 Zadpoor, A. A., "Mechanical meta-materials," pp. 371–381, 9 2016.

27 Kolken, H. M. and Zadpoor, A. A., "Auxetic mechanical metamaterials," pp. 5111–5129, 2017.

28 Ren, X., Das, R., Tran, P., Ngo, T. D., and Xie, Y. M., "Auxetic metamaterials and structures: A review," 1 2018.

29 Qu, J., Kadic, M., Naber, A., and Wegener, M., "Micro-Structured Two-Component 3D Metamaterials with Negative Thermal-Expansion Coefficient from Positive Constituents," *Scientific Reports*, vol. 7, 1 2017.

30 Wang, Y. C. and Lakes, R. S., "Extreme stiffness systems due to negative stiffness elements," *American Journal of Physics*, vol. 72, no. 1, pp. 40–50, 1 2004.

31 Smith, D. R. and Liu, R., "Metamaterials Tie Jun Cui," Tech. Rep.

32 Zhang, L., Wang, B., Song, B., Yao, Y., Choi, S. K., Yang, C., and Shi, Y., "3d printed biomimetic metamaterials with graded porosity and tapering topology for improved cell seeding and bone regeneration," *Bioactive Materials*, vol. 25, pp. 677–688, 7 2023.

33 Abbasi, N., Hamlet, S., Love, R. M., and Nguyen, N. T., "Porous scaffolds for bone regeneration," pp. 1–9, 3 2020.

34 Zhang, P., Liu, X., Guo, P., Li, X., He, Z., Li, Z., Stoddart, M. J., Grad, S., Tian, W., Chen, D., Zou, X., Zhou, Z., and Liu, S., "Effect of cyclic mechanical loading on immunoinflammatory microenvironment in biofabricating hydroxyapatite scaffold for bone regeneration," *Bioactive Materials*, vol. 6, pp. 3097–3108, 10 2021.

35 Matziolis, G., "Simulation of cell differentiation in fracture healingmechanically loaded composite scaffolds in a novel bioreactor system," *Bioactive Materials*, vol. 12, 2006.

36 Ravichandran, A., Lim, J., Chong, M. S. K., Wen, F., Liu, Y., Pillay, Y. T., Chan, J. K., and Teoh, S. H., "In vitro cyclic compressive loads potentiate early osteogenic events in engineered bone tissue," *Journal of Biomedical Materials Research - Part B Applied Biomaterials*, vol. 105, pp. 2366–2375, 11 2017.

37 Hippler, M., "3D Laser Lithography of Stimuli-Responsive Hydrogels," Tech. Rep., 2020.

38 Mirzaali, M. J., Pahlavani, H., Yarali, E., and Zadpoor, A. A., "Non-affinity in multi-material mechanical metamaterials," *Scientific Reports*, vol. 10, 12 2020.

39 Haq, M. A., Su, Y., and Wang, D., "Mechanical properties of PNIPAM based hydrogels: A review," pp. 842–855, 1 2017.

40 Peppas, N. A., Huang, Y., Torres-Lugo, M., Ward, J. H., and Zhang, J., "PHYSICOCHEMICAL FOUNDATIONS AND STRUCTURAL DESIGN OF HYDROGELS IN MEDICINE AND BIOLOGY," Tech. Rep., 2000. [Online]. Available: www.annualreviews.org

41 Mantha, S., Pillai, S., Khayambashi, P., Upadhyay, A., Zhang, Y., Tao, O., Pham, H. M., and Tran, S. D., "Smart hydrogels in tissue engineering and regenerative medicine," 10 2019.

42 Yasa, I. C., Tabak, A. F., Yasa, O., Ceylan, H., and Sitti, M., "3d-printed microrobotic transporters with recapitulated stem cell niche for programmable and active cell delivery," *Advanced Functional Materials*, vol. 29, 4 2019.

43 Belfield, K. D., Yao, S., and Bondar, M. V., "Two-photon absorbing photonic materials: From fundamentals to applications," pp. 97–156, 2008.

44 Infuehr, R., Pucher, N., Heller, C., Lichtenegger, H., Liska, R., Schmidt, V., Kuna, L., Haase, A., and Stampfl, J., "Functional polymers by two-photon 3D lithography," *Applied Surface Science*, vol. 254, no. 4, pp. 836–840, 12 2007.

45 Timoshenko, S., "Analysis of bi-metal thermostats."

46 Morimoto, T. and Ashida, F., "Temperature-responsive bending of a bilayer gel," *International Journal of Solids and Structures*, vol. 56, pp. 20–28, 3 2015.

47 Lucantonio, A., Nardinocchi, P., and Pezzulla, M., "Swelling-induced and controlled curving in layered gel beams," *Proceedings of the Royal Society A: Mathematical, Physical and Engineering Sciences*, vol. 470, 11 2014.

48 https://www.nanoscribe.com/en/.

49 Jin, D., Chen, Q., Huang, T. Y., Huang, J., Zhang, L., and Duan, H., "Four-dimensional direct laser writing of reconfigurable compound micromachines," *Materials Today*, vol. 32, pp. 19–25, 1 2020.

## VI. Appendix

### A. *Two-photon Polymerization*

Two-photon polymerization (2PP) (which comes under the realm of direct laser writing) is a printing technique used for the fabrication of dynamic structures both at the micro and nano-scale [13], [14]. 2PP requires the simultaneous absorption of two photons in a photosensitive material called photoresist to induce polymerization. This is in sharp contrast to other light-based photopolymerization techniques, where absorption of a single photon is sufficient to induce polymerization [43]. In 2PP, the photons that trigger the polymerization process are provided by a tightly focused femtosecond pulsated laser beam. Ti: sapphire lasers are usually preferred for inducing two-photon absorption (TPA) due to it's ability to produce ultrahigh peak power with a very short pulse width of approximately 100 femtoseconds.

Additionally, the central wavelength of Ti: sapphire lasers (which is about 800 nm) is approximately equal to half the wavelength of polymerization. As a result, the threshold energy for polymerization can be easily controlled, thus allowing for high spatial resolution of the printed structure [15]. The smallest feature that can be printed using 2PP is called a voxel. The size of a voxel is influenced by factors such as the properties of the photoresist material and the characteristics of the laser used. **Figure. 6** provides an illustration of 2PP.

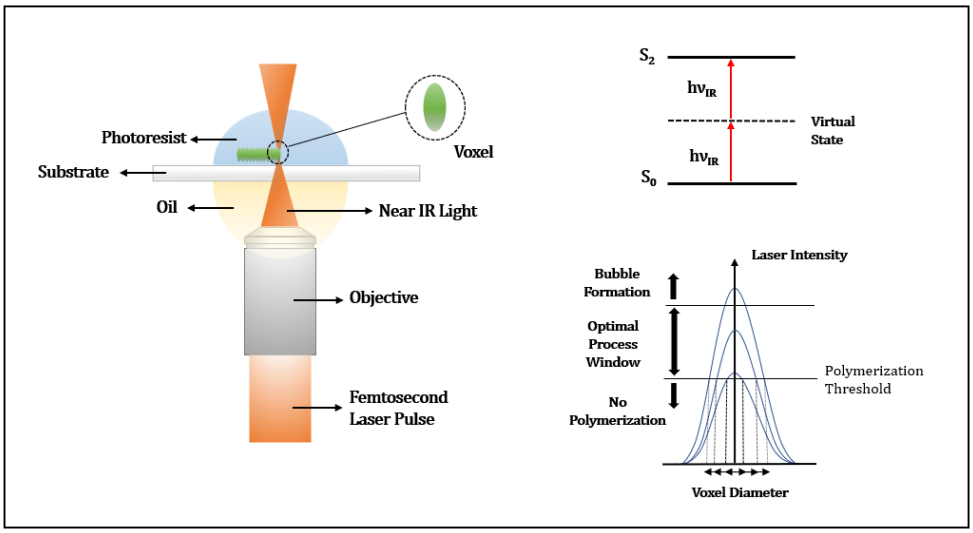


Fig. 6: Overview of two-photon polymerization and influence of laser intensity on voxel diameter

The liquid-state photocurable resin used in 2PP is transparent to near-infrared (NIR) light. Most polymers used in 2PP exhibit a linear absorption in the near-infrared zone thus allowing the laser to penetrate deeply into the material. This is one of the key factors that enables the 2PP process to create complex nanostructures with excellent spatial resolution.

A photoresist consists of four main components, namely the monomer, photoinitiator, cross-linker, and base solvent [44]. The relative proportions of each of these components determine the properties of the structure being printed. On exposure to the femtosecond laser, rapid polymerization of the photoresist occurs through four stages. The first stage involves the formation of a radical, which leads to the initiation of chain formation followed by its propagation. There is a point during the polymerization process where two radically active polymer chains combine to form a single chain, thus resulting in chain termination [37]. A brief overview of the polymerization process associated with 2PP is illustrated in **Figure. 7**.

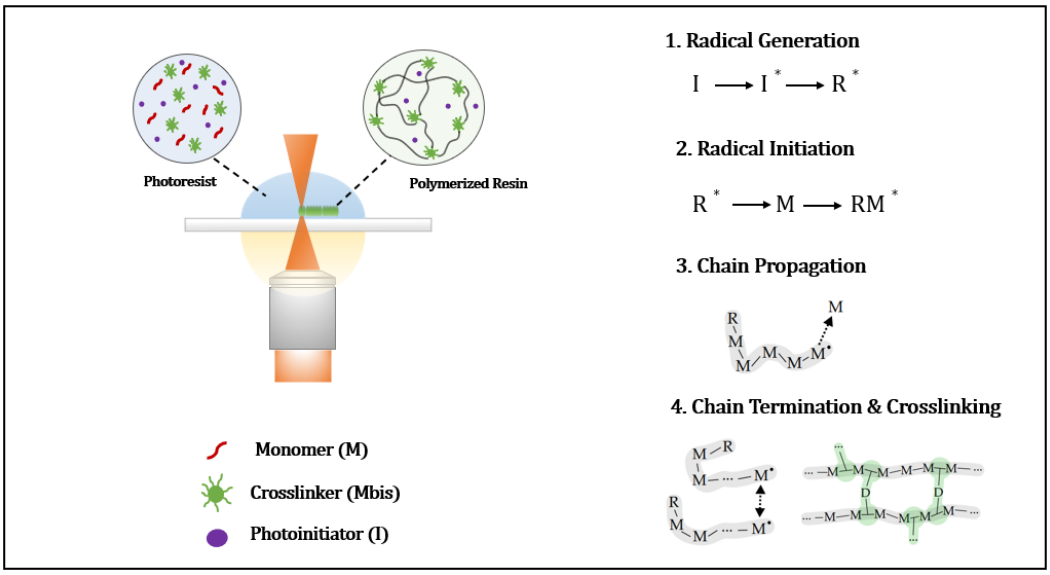


Fig. 7: Overview of the four steps of polymerization during fabrication of structures using 2PP [37]

### *B. Hydrogel-Based Photoresists*

*1) **Overview of Hydrogels**:* Hydrogels are materials that are capable of absorbing and retaining large amounts of water or other aqueous solutions, thereby undergoing significant swelling. This is made possible due to the hydrophilic polymer chains that constitute the hydrogel matrix. The polymer chains contain functional groups that form hydrogen bonds with the water molecules, thus allowing for absorbing and retaining large amounts of water. Additionally, the polymer chains constituting the hydrogel matrix are crosslinked, creating a three-dimensional network that traps water molecules within the interconnected voids. When hydrogels are subjected to a temperature change, the polymer chains transition from a hydrophilic to a hydrophobic state, resulting in water being expelled out of the hydrogel matrix, thereby causing the material to shrink. It is to be noted that this transition is reversible and the material gains back its hydrophilic nature once the external stimulus is removed. An illustration of the above concept is depicted in **Figure. 8.a**.

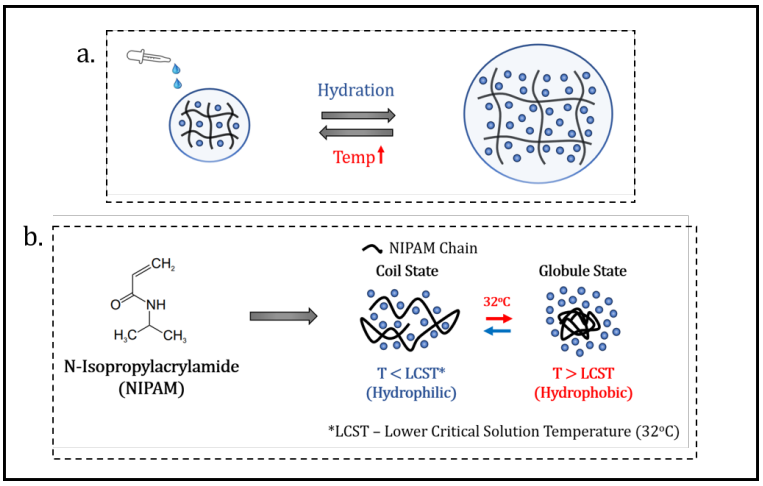


Fig. 8: Shape-morphing in hydrogels. (a) Reversible swelling and shrinking of hydrogels when subjected to temperature change. (b) Coil-to-globule transition of pNIPAM chain when the temperature is increased above LCST [37]

Poly(N-isopropylacrylamide)-based hydrogels are one class of hydrogels that are widely used, especially in combination with 2PP, for the fabrication of stimuli-responsive structures. NIPAM monomers, when polymerized during 2PP printing, form pNIPAM chains that exhibit hydrophilic characteristics at room temperature. However, when the temperature is increased beyond the lower critical solution temperature (LCST) of NIPAM, which is about 32 °C, pNIPAM exhibits a hydrophobic behavior, thus undergoing a large discontinuous volume change as illustrated in **Figure. 8.b**. This transition from a hydrophobic

to a hydrophilic state is completely reversible, and the polymer chain returns to its original configuration once the thermal stimulus is removed [17]. Since the LCST of pNIPAM is very close to the human body temperature and owing to its good biocompatibility, PNIPAM-based structures find widespread applications in the field of biomedicine [18].

*2) **Thermodynamic Overview of Coil to Globe Transition in pNIPAM Chain**:* As mentioned earlier, pNIPAM chains are soluble in water below the LCST. This is because the water molecules form hydrogen bonds with the polar regions of the polymer, thus resulting in a negative exothermic enthalpy $\Delta$H. The alignment and reorientation of water molecules also results in a negative entropy $\Delta$S for the system. When viewed in terms of the Gibbs free energy of the system expressed as:

$$\Delta G = \Delta H - T\Delta S$$

The realignment of water molecules at room temperature results in a negative value of $\Delta$G as the $\Delta$H term dominates. This indicates that it is thermodynamically more favorable for water molecules to form hydrogen bonds with the polymer chain. However, when the temperature is increased beyond the LCST, the term '-T$\Delta$S' dominates and eventually the value of $\Delta$G becomes positive. This results in the breaking of hydrogen bonds formed between the water molecules and the polymer chains thus leading to phase separation. This explains the abrupt transition of the polymer chain from a coil to a globe state at 32°C. Further details on the chemistry and thermodynamics behind the phase transition of pNIPAM can be found in literature [37].

However, when it comes to hydrogel network, the cross-linkers present in the medium serve as connecting links between individual polymer chains, thus ensuring that individual chains do not transform into the globule state when the material is subjected to a temperature above the LCST. As a result each polymer chain partially curls up, thereby expelling the water from the matrix. This results in an isotropic shrinkage of the material. It is to be noted that the shrinkage of the matrix is also accompanied by changes in its mechanical properties such as stiffness. As the temperature is decreased below the LCST, the hydrogel matrix again forms hydrogen bonds with the water molecules and swells up, thus making the entire process reversible.

*3) **Microfabrication of Hydrogel-Based Structures**:* pNIPAM-based photoresists are widely used in combination with 2PP to fabricate stimuli-responsive microstructures [16]. The amount of water that a hydrogel-based structure fabricated using 2PP can hold largely depends upon the extent of cross-linking between the polymer chains within the hydrogel matrix. The extent of cross-linking in a hydrogel-based microstructure is directly dependent on the printing parameters, particularly the laser power and laser scanning speeds, and follows a trend as depicted in the relationships given below.

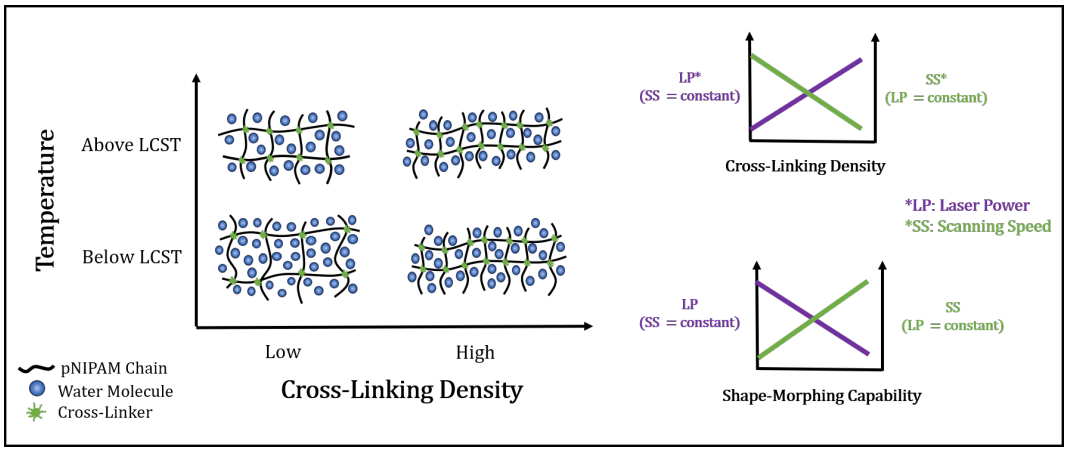


Fig. 9: Relation between printing parameters and cross-linking densities in pNIPAM-based microstructures

$$\text{Cross-Linking Density} \propto \text{Laser Power} \tag{1}$$

$$\text{Cross-linking Density} \propto \frac{1}{\text{Scanning Speed}} \tag{2}$$

$$\text{Cross-linking Density} \propto \frac{1}{\text{Shape-Morphing Ability}} \tag{3}$$

An increased cross-linking density directly translates to a polymer matrix characterized by multiple interconnections between the polymer chains, thus resulting in a reduced capacity for water absorption or expulsion. Consequently, the level of deformation that a highly cross-linked section can undergo when exposed to a thermal stimulus is reduced as compared to a polymer matrix with a lower cross-linking density. An illustrative representation of the above concept in relation to the pNIPAM-based hydrogel matrix is as shown in **Figure. 9**.

Utilizing this shape-morphing capability of pNIPAM-based hydrogel material, and combining it with suitable printing parameters, microstructures capable of exhibiting complex shape-morphing behavior can be fabricated.

### *C. Mathematical Overview of Deformation in Bi-layered Hydrogel Structures*

The Timoshenko beam model (linear) [45] is adopted to understand the directional bending of the bi-layered hydrogel beam from a mathematical perspective. An illustration of the shrinkage-induced bending of the bi-layered beam is shown in **Figure. 10**.

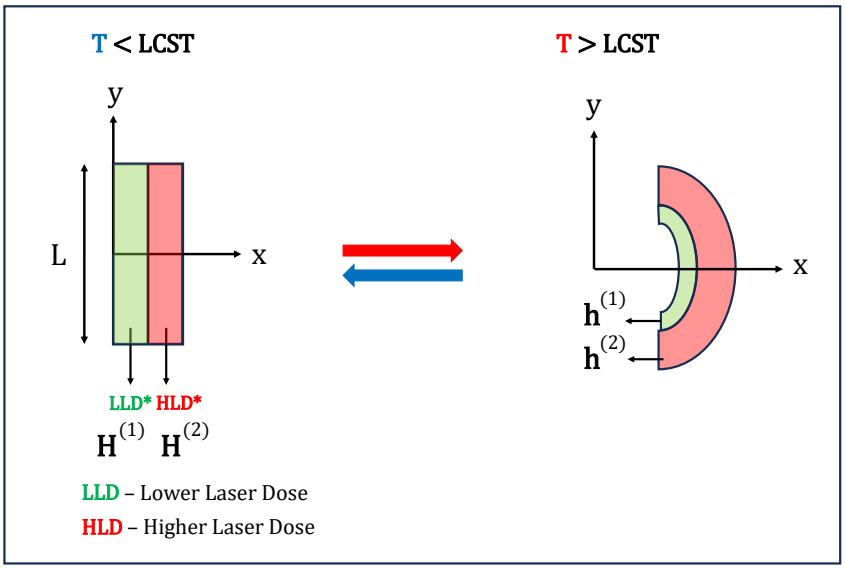


Fig. 10: Schematic illustration of shrinkage-induced bending of bi-layered hydrogel structures due to different shrinkage ratios when subjected to a thermal stimulus above LCST

Here, $H^{(1)}$ and $H^{(2)}$ correspond to the thickness of the lower and higher polymerized sections of the beam respectively. The principle strains along the three axes obtained from Hooke's law is as follows:

$$\epsilon_x = \frac{1}{E}[-\upsilon(\sigma_z + \sigma_x)] \tag{4}$$

$$\epsilon_y = \frac{1}{E}[\sigma_x - \upsilon\sigma_z] + \epsilon_o \tag{5}$$

$$\epsilon_z = \frac{1}{E}[\sigma_z - \upsilon(\sigma_x + \sigma_y)] + \epsilon_o \tag{6}$$

where $\epsilon_x$, $\epsilon_y$, $\epsilon_z$ correspond to the principal strains along the x,y,z axis respectively, while $\sigma_x$, $\sigma_y$, $\sigma_z$ correspond to the principal stress along these axes. The term $\epsilon_o$ in the equations above refers to the strain in the structure as a result of inhomogeneous shrinkage. The principal strain in the z-direction ($\epsilon_z$) is independent of the position throughout the thickness of the beam. For simplicity, an assumption is made that the stress along the x-direction is close to zero, i.e, $\sigma_x \approx 0$, assuming that the thickness of the bi-layer beam is very thin compared to the length of the beam. However, for the dimensions of the beam considered in this research, this assumption is only partially valid, as the width of the beam is not negligible compared to the length of the

beam. To get a more precise estimate of the deformation of the beam, a finite beam theory based on finite elasticity should be used as mentioned in literature [46]. Substituting $\sigma_x$ = 0 in equations 4, 5, 6 yields:

$$\epsilon_x = -\frac{1}{E}\upsilon\sigma_z \tag{7}$$

$$\epsilon_y = -\frac{1}{E}\upsilon\sigma_z + \epsilon_o \tag{8}$$

$$\epsilon_z = \frac{1}{E}[\sigma_z - \upsilon\sigma_y] + \epsilon_o \tag{9}$$

Bending strain along the y-direction [46] is expressed as:

$$\epsilon_y = c + \frac{x - x_b}{R} \tag{10}$$

where 'c' is a constant and $x_b$ corresponds to the position of the plane where there is no bending strain. Using equation 10 and solving for $\sigma_y$ using equations 7, 8, 9, followed by computing the force balance equations (uniform strain, bending strain, and bending moment with respect to the bending axis) gives the following relation for the bending curvature

$$\frac{1}{R} = \frac{6[(1+\upsilon^{(2)})\varepsilon_0^{(2)} - (1+\upsilon^{(1)})\varepsilon_0^{(1)}]}{h^{(1)}} \times \frac{[(1-\eta\delta^2)^2 + 4\eta\delta(1+\delta)^2]}{\eta\delta(1+\delta)} \tag{11}$$

where $\eta = \widehat{E}^{(2)}/\widehat{E}^{(1)}[\widehat{E} = E/(1-\upsilon^2)]$ and $\delta = h^{(2)}/h^{(1)}$. It is to be noted here that these expressions have been reported by Timoshenko for a bi-metal strip [45]. Additional details pertaining to the above derivation can be found in literature [46]. For further insights into the mathematics behind the directional deformation of bi-layered structures, the following literature can be referred to [47].

It is important to emphasize here that the expressions obtained are only used to understand the relationships between the elastic modulus ($E$) and the thickness of each segment of the bi-layered beam on its deflection. For a more comprehensive understanding of the deformation of bi-layered hydrogel beams, an extensive and detailed model is required, and is out of the scope of this thesis.

### *D. Photoresist Composition and Preparation*

| Component | Chemical Name | Quantity |
|---|---|---|
| Thermo-responsive Monomer | N-isopropyl-acrylamide (NIPAM) | 400 mg |
| Photo-initiator | lithium phenyl(2,4,6-trimethyl-benzoyl)phosphinate (LAP) | 15 mg |
| Cross-linker | N,N'-methylenebis(acrylamide) (Mbis) | 40 mg |
| Solvent | Ethylene glycol | 450 µL |

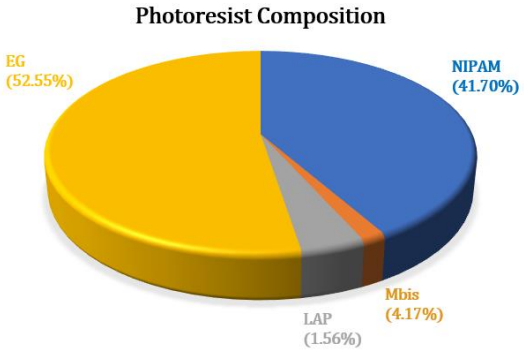


Fig. 11: Composition of photoresist and corresponding weight percentage of each constituent of the photoresist solution

A step-by-step procedure to prepare the photoresist solution is as shown in **Figure. 12**.

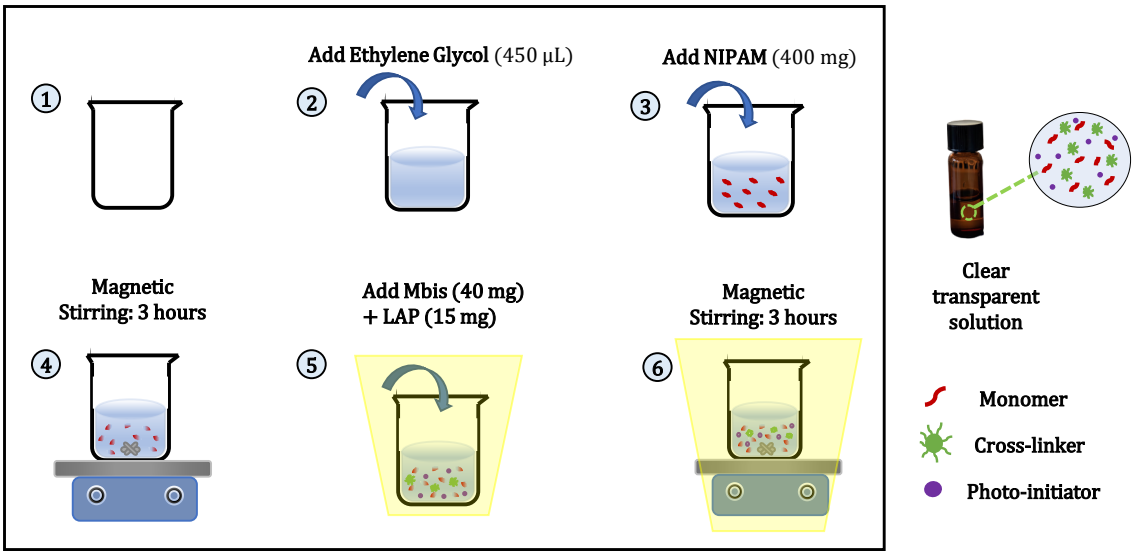


Fig. 12: Step-by-step approach for preparation of pNIPAM-based photoresist

## *E. Overview of Setup for Two-Photon Polymerization Printing*

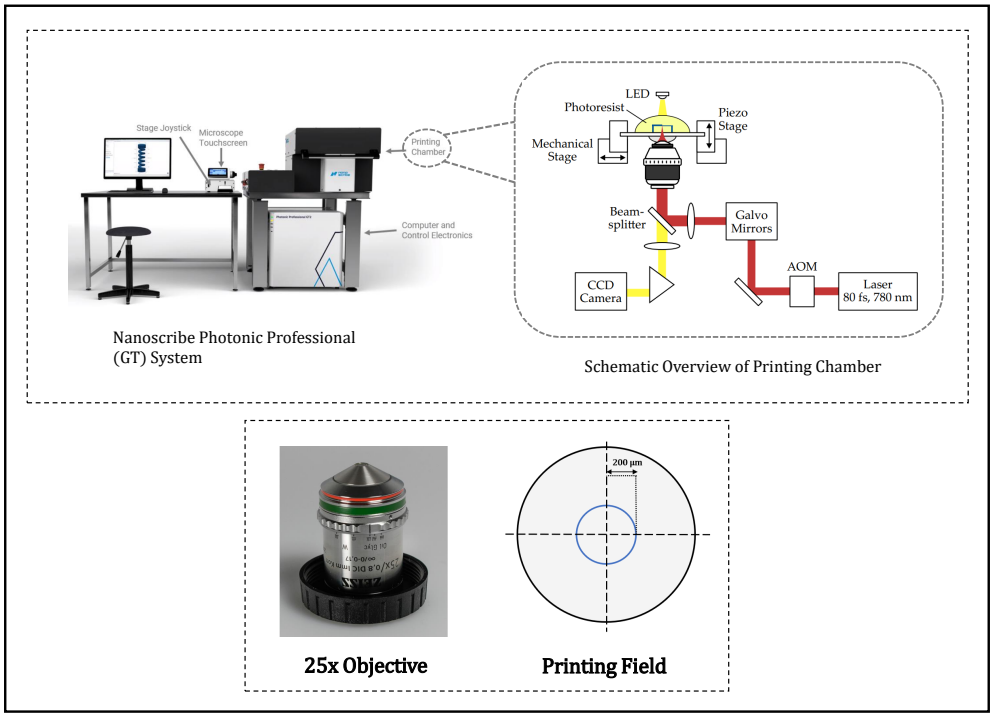


Fig. 13: Illustration of the printing chamber of Nanoscribe Photonic Professional GT and the objective used for printing the microstructures [37], [48]

TABLE I: Specifications of the objective used for printing the microstructures [48]

| Parameters | Value |
|---|---|
| Objective | 25x NA 0.8 |
| Immersion Media (Mode) | Oil |
| Working Distance (WD) | 380 µm |
| Objective Opening Angle (a) | 31° |
| Objective Lens Diameter (D) | 5.2 mm |
| Printing Field (Galvo Mode) | 400 µm |
| Theoretical Lateral Resolution | 595 nm |
| Theoretical Axial Resolution | 3313 nm |
| $\Delta$N required @ 830nm | >0.1 |

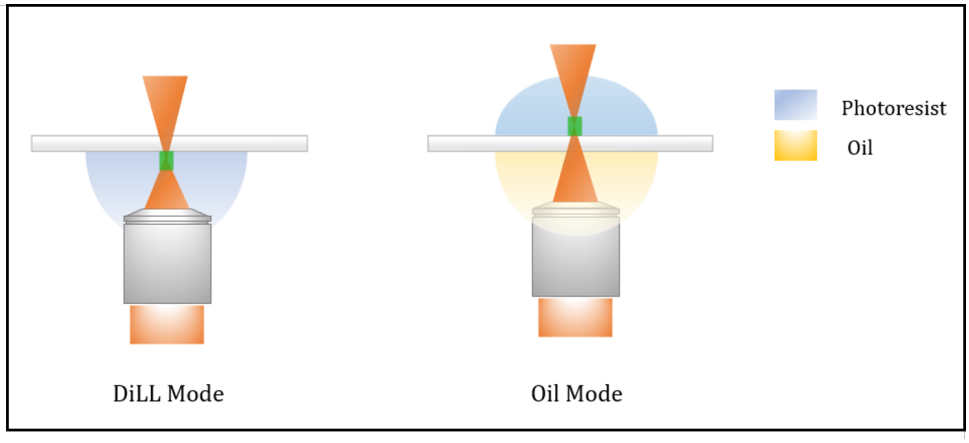


Fig. 14: Illustration of the two printing modes that can be used for fabricating structures in the Nanoscribe Photonic Professional GT. In the DiLL (Dip in Laser Lithography) mode, the objective is directly immersed in the photoresist and the structures are printed top-down. In the oil mode, the objective is immersed in an oil and the femtosecond laser passes through the oil and substrate before it enters the photoresist and initiates the polymerization reaction. Due to the thickness of the substate, the maximum height that can be printed in the oil mode is slightly lesser than the DiLL mode

### *F. Silanization of Glass Substrates*

All glass substrates on which the microstructures are printed are made to undergo silanization. Silanization is a surface treatment process used to modify the surface properties of the glass substrate. A brief overview of the entire process adopted to prepare the glass substrate for printing is as follows: First, the glass substrate is cleaned using acetone and isopropanol. Next, the glass substrate is made to undergo oxygen plasma treatment. In this step, the samples are placed in a vacuum chamber and oxygen gas is introduced into it. Upon energising the chamber, oxygen plasma is created. The plasma contains highly reactive oxygen radicals and ions. When this plasma is exposed to the glass surface, it results in the formation of silanol (Si-OH) groups on the surface of glass.

Following oxygen plasma treatment, the glass substrate is immediately exposed to a solution of 3-(Trimethoxysilyl)propyl Methacrylate (>98%). This solution contains silane coupling agents, and these react with the silanol (Si-OH) groups already present on the glass surface, thus forming strong chemical bonds. This leads to the formation of a silane monolayer on the glass surface. This monolayer significantly modifies the properties of the glass surface, introducing properties that are suitable and desirable for 2PP. The hydrophobic behaviour of the glass substrate is one such property. The hydrophobic surface causes the photoresist liquid to form distinct droplets, thereby minimizing spreading, and is as illustrated in **Figure.15**. Additionally, the monolayer forms covalent bonds between the printed structure, thus ensuring that it adheres firmly to the substrate. This is important during the development phase, as it prevents delamination and dislodging of the structure.

For all the experimentations performed in this thesis, the glass substrates were exposed to the oxygen plasma for 15 minutes,

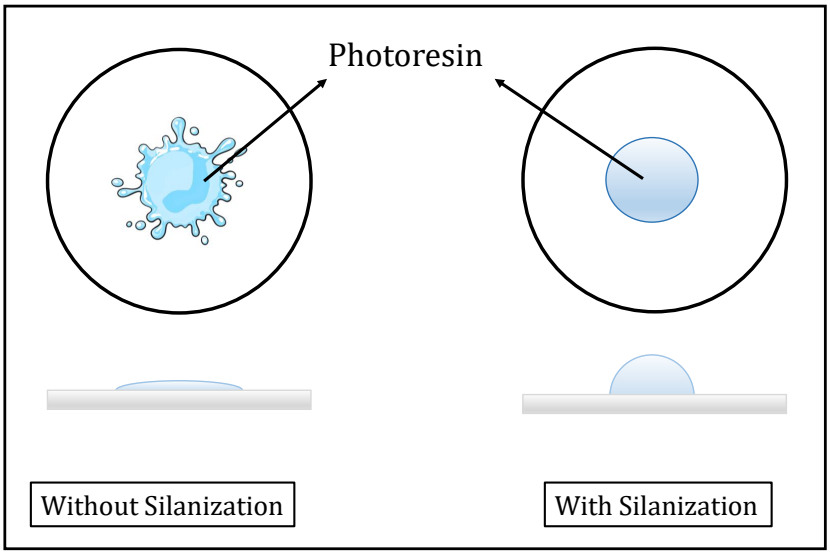


Fig. 15: Influence of silanization on the surface properties of glass substrates

followed by silanization for 1 hour. One observation made while preparing the glass substrate prior to printing is that it is favourable to clean the silanized glass samples only with isopropanol, and not use both isopropanol and acetone to clean the samples. The reason behind this is that cleaning only with isopropanol makes it easier to detect the interface between the glass substrate and the photoresist during printing.

### *G. Overview of Procedure from Design to Fabrication*

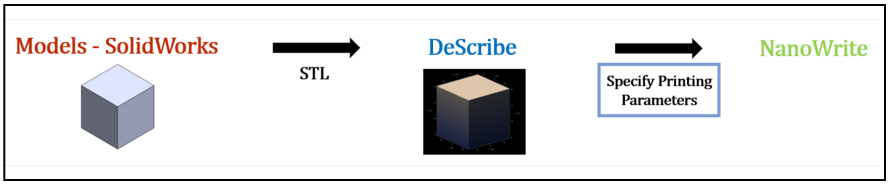


Fig. 16: Illustration of the procedure from modeling the proposed structures to its fabrication

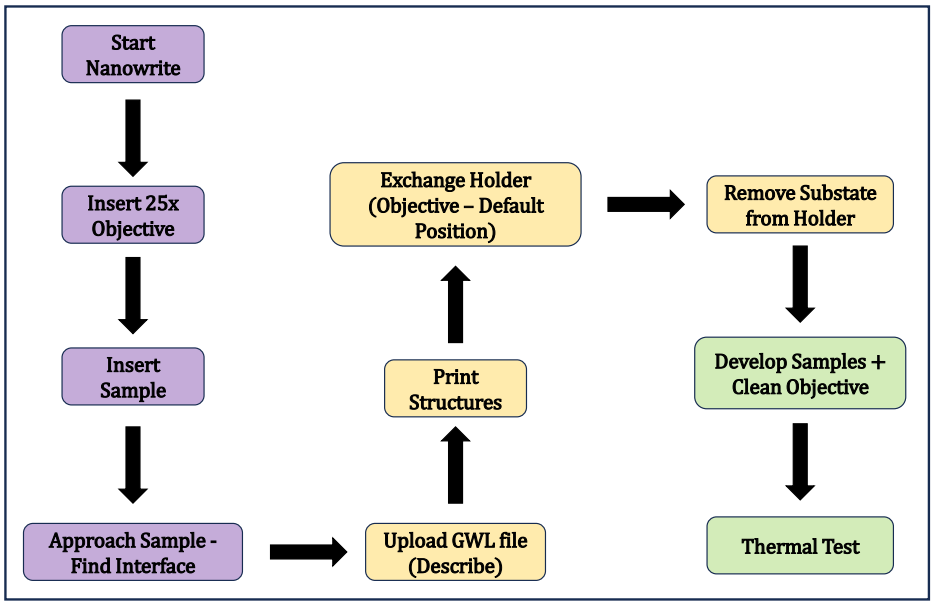


Fig. 17: Workflow from setting up the Nanoscribe printer to conducting thermal tests

### *H. Post-fabrication Development Procedure*

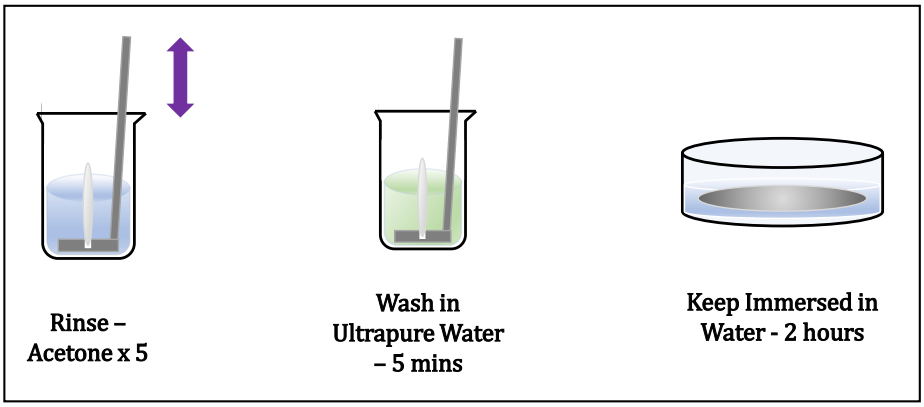


Fig. 18: Illustration of the post-fabrication procedure adopted to develop the samples before conducting thermal tests

### *1. Experimental Setup for Optical Characterization*

*1)* ***Microscope Setup****:* An Olympus CKX 53 microscope is used for carrying out optical characterizations of the printed structures when subjected to a thermal stimulus and is as shown in **Figure.19**.

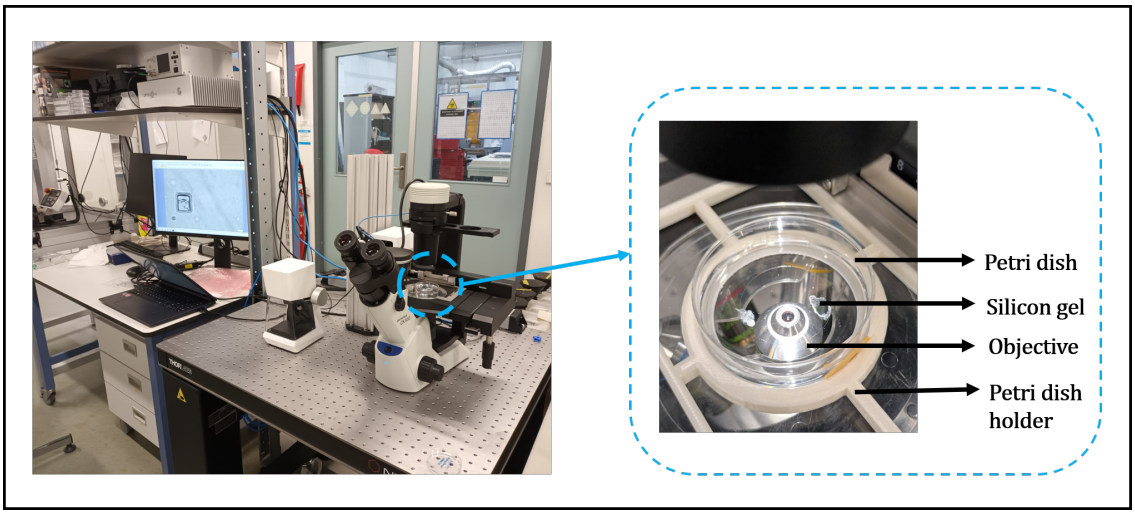


Fig. 19: The setup used for optical characterization of the printed microstructures

The Petri dish containing the sample is placed in an appropriate position as shown in the Figure. It is to be noted here that the microscope has an objective at the underneath. This is ideal for evaluating the samples during thermal tests, as the vapors of hot water do not come in contact with the objective, thus ensuring that no damage is caused to the objective. The sample is held in place within the Petri dish using silicon as shown in **Figure.19**. This ensures that the glass substrate containing the samples does not float around in the water. A 3D-printed holder is fabricated to hold the Petri dish in place.

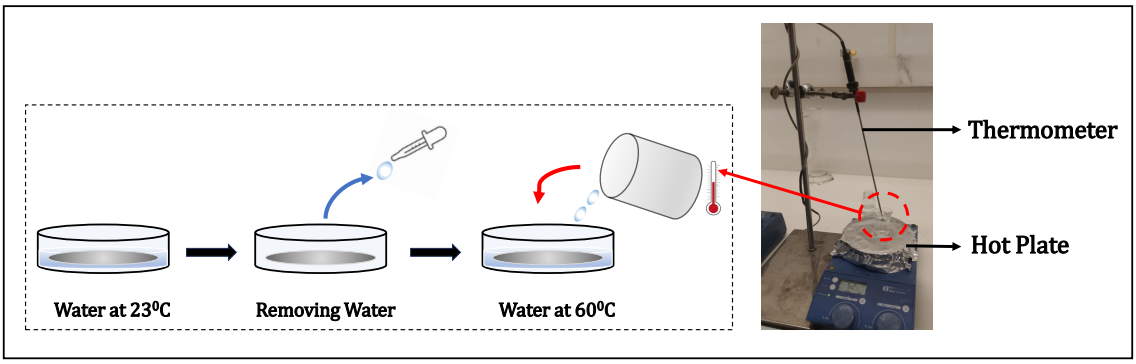


Fig. 20: Illustration of the procedure adopted to provide thermal stimulus to the microstructures

*2)* ***Thermal Stimulus****:* In a typical thermal test, water is heated in a beaker using the hot plate in the lab. Once the water reaches the desired temperature, it is poured into the Petri dish, and the deformations of the structures are observed and recorded using the live feed obtained on the monitor placed next to the microscope setup. **Figure.20** depicts the steps taken to provide a thermal stimulus to the printed microstructures.

### *J. Dose Test*

A 11x11 matrix of cuboids (20 x 20 x 15 µm) was printed to characterize the photoresist and determine the printer parameters that suit best for the given photoresist composition. An illustration of the dose test performed is as shown below:

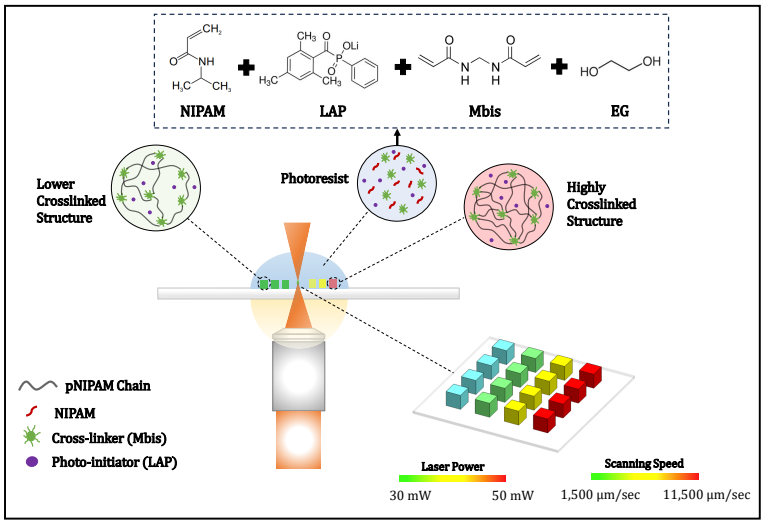


Fig. 21: Overview of dose test performed to characterize the photoresist and evaluate the influence of printing parameters on the extent of polymerization

It is evident from the results of the dose test (**Figure.22**) that blocks printed with low scanning speeds result in over-polymerization within the photoresist and thus the structures are burnt. However, for a given laser power, as the scanning speed is increased, the extent of polymerization reduces and in some cases, there is minimal polymerization that occurs in the photoresist.

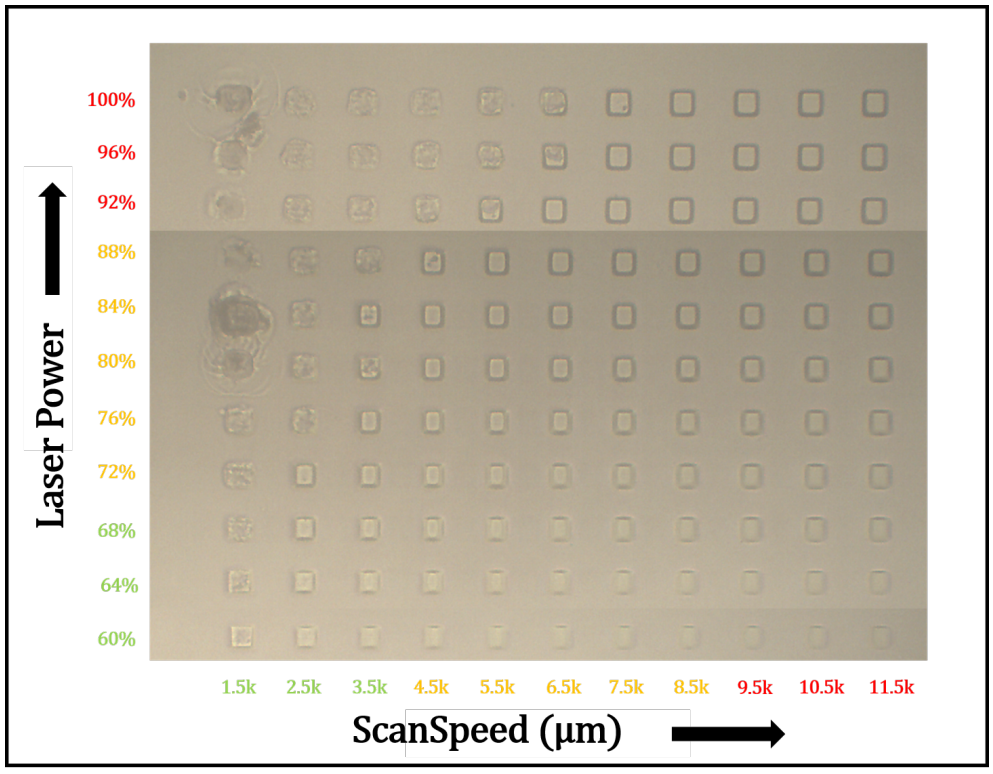


Fig. 22: Results of dose test

The structures towards the top right section of the figure are structurally well-defined, thus making the corresponding range of laser power and scanning speeds suitable for this research. It is to be noted that in order to assess the extent of polymerization quantitatively, nanoindentation tests need to be performed and the stiffness of each block must be recorded. A larger stiffness corresponds to a higher degree of polymerization and this can be used as a basis to evaluate if the laser power or the scanning speed has a greater impact on the extent of polymerization.

### *K. Residual Stress in Fabricated Microstructures*

Following fabrication, some microstructures were present in an unintended deformed state as seen in **Figure.23**. One possible reason for this could be due to the residual stresses in the structure. Numerous factors could have possibly contributed to the formation of residual stresses within the printed microstructures. The femtosecond laser used to print the microstructures causes localized heating within the photoresist, which in turn results in localized thermal gradients being formed, which could possibly lead to residual stresses in the printed structures. Additionally, once the process of polymerization is complete, the differing rates of cooling within the differently polymerized sections could also contribute to residual stresses. Furthermore, the printing process used to fabricate the structures involves layer-by-layer printing, where the newly polymerized layer may encounter strain restriction from the adjacent layers that have already solidified. This can further contribute to the development of residual stresses within the structure.

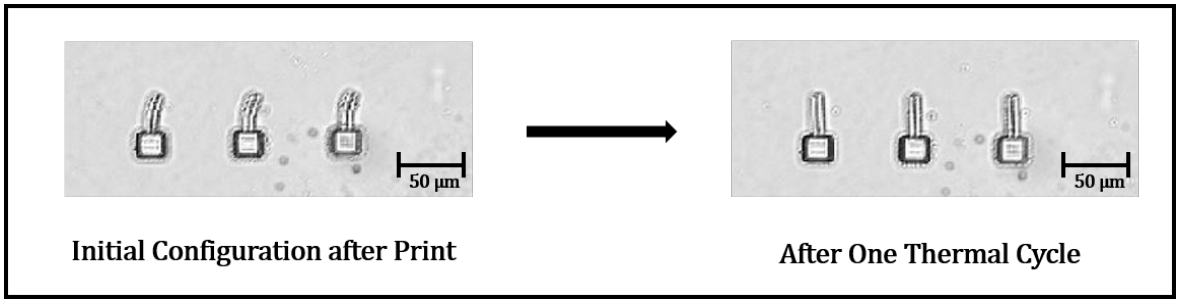


Fig. 23: Eliminating residual stresses from fabricated microstructures by stress-relieving annealing

To eliminate residual stresses, a stress-relieving annealing process is employed. During this process, the microstructures are placed in water at a temperature of approximately 60°C, followed by gradual cooling to room temperature. This process causes the structures to return to their original intended configuration as seen in **Figure.23**. One possible reason for this behavior could be the reorientation of the polymer chains within the structure, leading to a redistribution of stress resulting in relaxation of the material to its intended state.

### *L. Evaluating Overlap Between Beam Elements*

In order to print the desired bi-layered microcantilever beams, determining an optimal design and printing strategy is equally important as selecting the right laser printing parameters. Here, two main design considerations, namely the overlap between the different layers of the beam element, and the overlap between the beam and the post are discussed (**Figure.24**).

An optimal overlap between the two layers of the cantilever beam is essential to ensure that the two layers do not delaminate when subjected to a thermal stimulus. Characterizations were performed where the extent of overlap (between the two beam segments) was varied between 0.55 µm and 0.95 µm, and the angular displacements of the beam were recorded when subjected to a thermal stimulus. The results obtained **(Case A – Figure.24)** indicate that an overlap of 0.75 µm provides a right balance between shape-morphing behavior and structural stability of the beam element. A value of overlap lower than 0.75 µm causes the two layers to delaminate when subjected to repeated cycles of thermal stimulus (3 cycles in this case). Increasing the overlap beyond 0.75 µm causes the beam element to be more structurally stable and rigid, thereby simultaneously reducing the extent of deformation the beam displays when subjected to a thermal stimulus. Thus, an overlap of 0.75 µm between the two layers of the beam segment was chosen to print all bi-layered structures in this thesis.

Next, it was also important to determine the optimal overlap between the beam and the post **(Case B – Figure.24)**. A larger overlap causes local burning (due to over-polymerization) at the interface between the beam and post, while a smaller value of overlap causes the beam to either delaminate from the post, or in some cases even break away (if beams of large dimensions

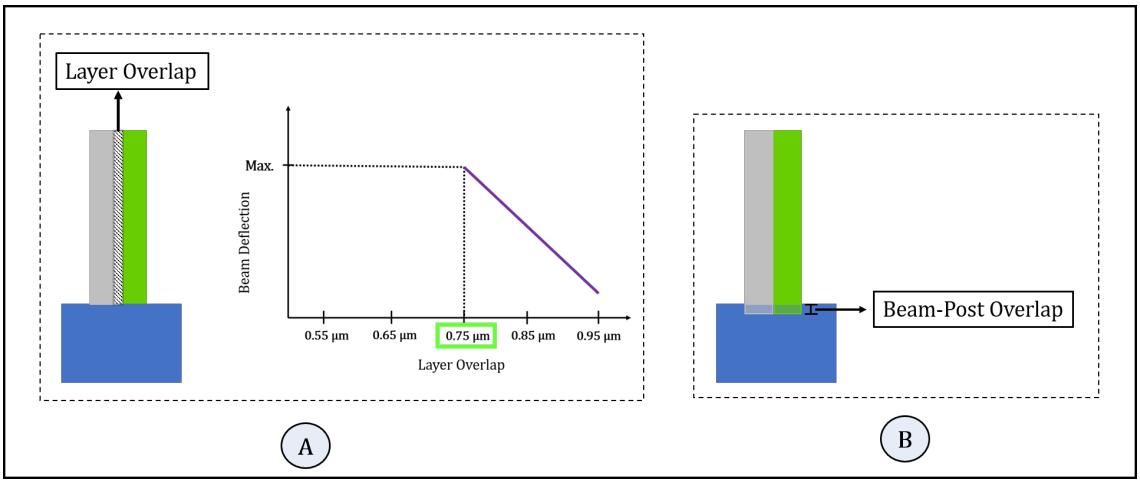


Fig. 24: Illustration of characterizing the overlap between beam elements

are printed). After evaluating different values of overlaps in the range of 0.5 µm to 3 µm, a value of 2 µm was chosen. It is to be noted here that the choice of printing parameters also plays an important role determining the optimal overlap between structures. Given the choice of laser power (100% and 85%) and the scanning speed (8000 µm /sec), an overlap of 2 µm was the optimal choice in this case. The overlap between all structural elements of the final proposed design was also kept fixed at a value of 2 µm.

### *M. Shrinkage Characterization*

The sample set used to characterize the shrinkage in the structures as a function of laser power is as shown in **Figure.25**.

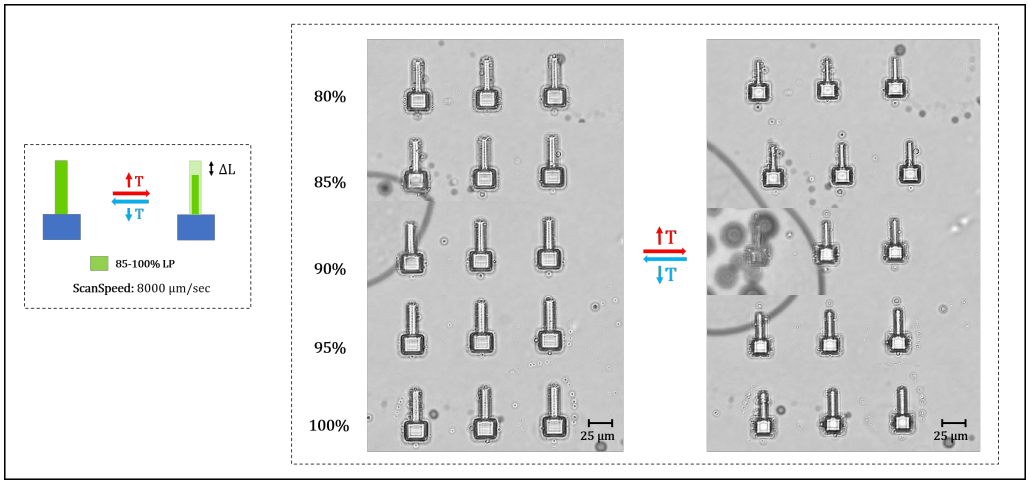


Fig. 25: Sample set used to characterize the extent of shrinkage of beam elements as a function of laser power

The extent of shrinkage for each case (along the length of the beam) is evaluated by taking the average between the three samples. The corresponding values of standard deviation are also calculated and a plot is made to depict the relationship between laser power and shrinkage.

### N. *Characterizing Coefficient of Thermal Expansion for Beam Elements*

The coefficient of thermal expansion (CTE) for the beam elements was calculated based on the observed change in its length when subjected to a thermal stimulus. Here, the aim was to determine the relation between the laser power used to fabricate the cantilever beams and the corresponding change in the material's response to the applied thermal stimulus. The CTE was calculated using the relation:

$$\alpha = \Delta L/(L_0 \times \Delta T) \tag{12}$$

where $\alpha$, $\Delta L$, $L_0$, and $\Delta T$ correspond to the CTE, change in length of the beam when subjected to a thermal stimulus, the original length of the beam, and the change in temperature respectively. The results obtained are shown in **Figure.26**.

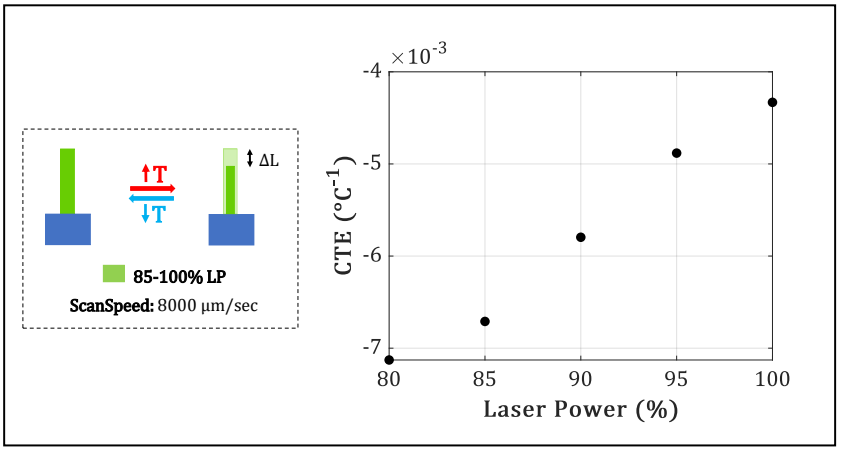


Fig. 26: Influence of laser power on the coefficient of thermal expansion of beam elements

It is to be noted here that the CTE is a negative value, indicating that the material shrinks instead of expanding when subjected to a change in temperature. The results obtained indicate a near linear (and inversely proportional) relationship between the laser power and CTE.

An additional characterization was performed to evaluate the change in area of the beam when subjected to a temperature change and is as shown in **Figure.27**.

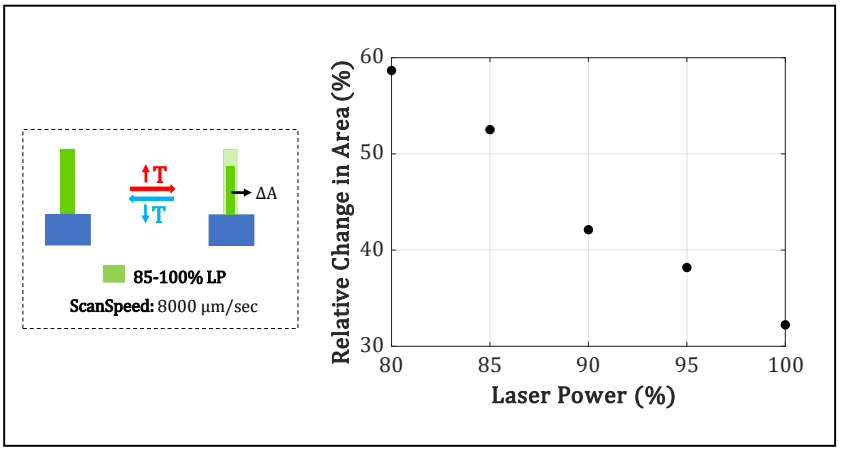


Fig. 27: Influence of laser power on the change in the area of beam elements (length x width)

The results obtained in this section hold significance while developing simulation models for characterizing beam deformation.

### O. *Influence of Laser Power Combination on Angular Deflection of Beams*

The sample set used to characterize the influence of laser power combination on beam deflection is as shown in **Figure.28**.

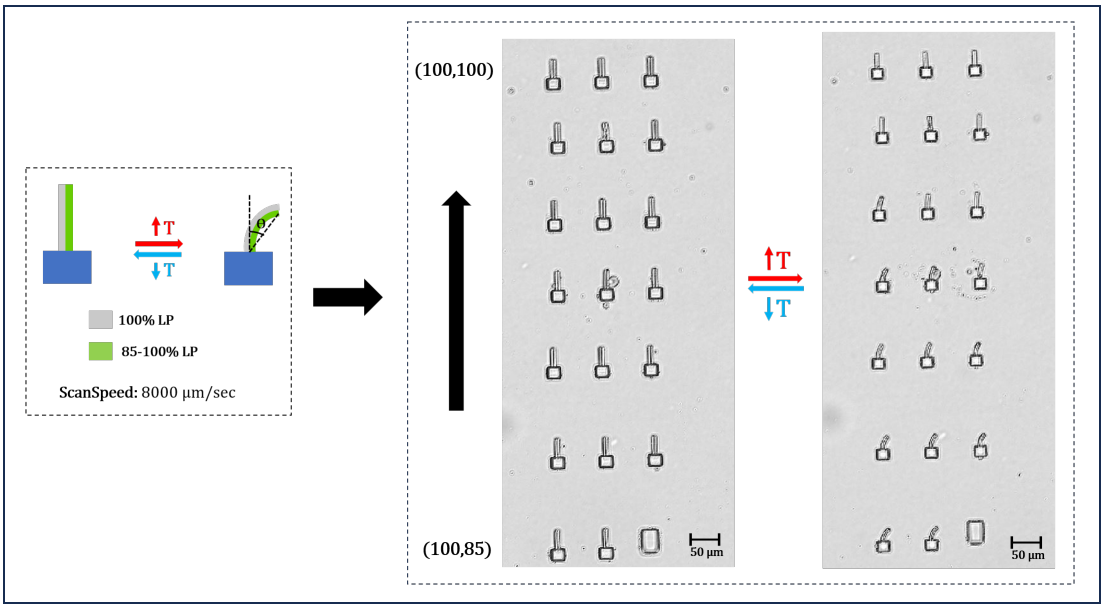


Fig. 28: Sample set used to characterize the angular deflection of beams as a function of laser power combination

In the bi-layered structure, one segment of the beam was printed using a constant laser power set at 100%. The laser power for the other segment was varied from 85% to 100% in increments of approximately 3%. The scanning speed used to print the structures was kept constant at 8000 µm/sec.

### P. *Influence of Scanning Speed on Angular Deflection of Beams*

The sample set used to characterize the influence of scanning speed on the angular deflection of beams is as shown in **Figure.29**.

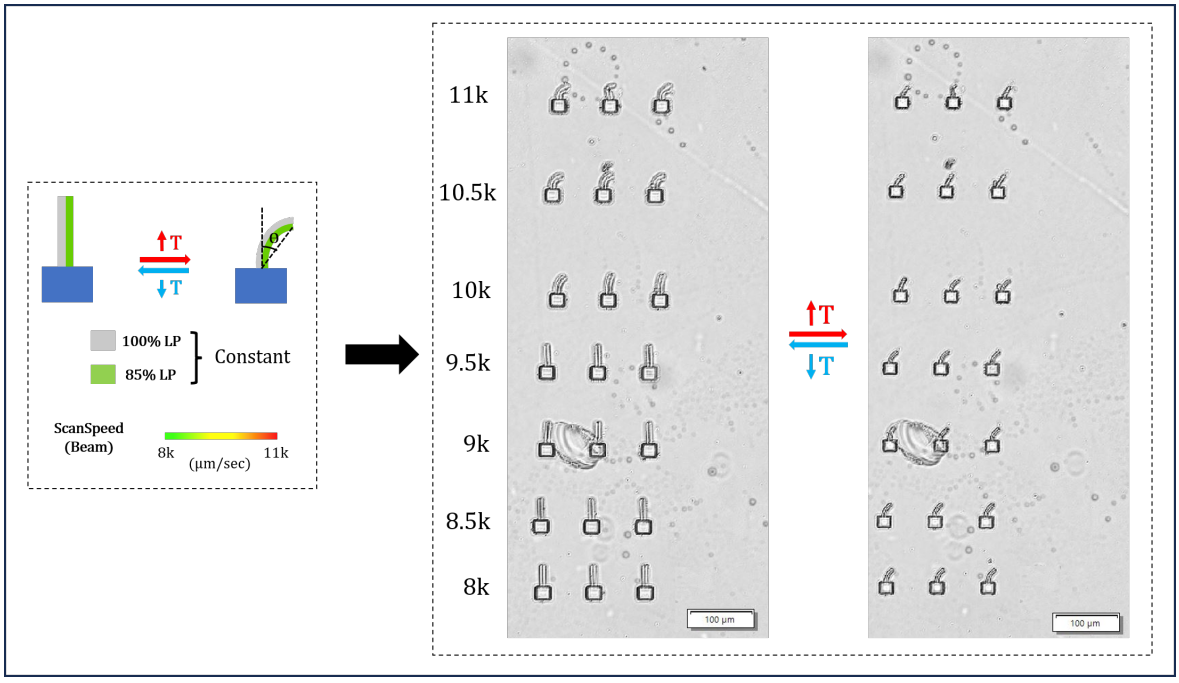


Fig. 29: Sample set used to characterize the angular deflection of beams as a function of scanning speed

As seen in the figure, a scanning speed beyond 10,000 µm/sec is not sufficient enough to polymerize the photoresist adequately to obtain the desired bi-layered beam. It is to be noted here that though a scanning speed above 10,000 µm/sec can be used to print microstructures as evident from the dose test (**Figure.22**), printing complex geometries at this scanning speed becomes a challenge. Thus, it can be concluded that both geometry and printing parameters influence the printability and shape-morphing behavior of a structure.

### *Q. Influence of Hatching Angle on Angular Deflection of Beams*

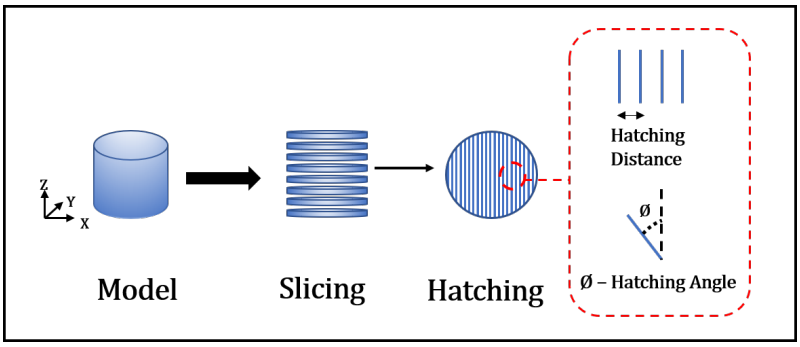


Fig. 30: Schematic representation of hatching

*1) **Overview of Hatching**:* An illustration of splitting a designed part into multiple slices,where each slice is further hatched into multiple segments is as shown in **Figure.30**.

In this thesis, the influence of hatching angle on the shape-morphing behavior of the microstructures was explored in detail. In addition to the hatching angle characterizations illustrated in the 'Results and Discussion' section of the paper, further characterizations were also performed to get a better understanding of the influence of hatching angle on the shape-morphing behavior of the desired structures, and is as illustrated in the section below.

*2) **Influnce of Hatching Angle on Beam Deformation**:* The microstructures used to evaluate the influence of hatching angles on the angular deflection of the beams are as shown in **Figure.31** and **Figure.32**. A thermal stimulus of 60°C was provided to induce the deformations. The beams were subjected to three thermal cycles, and the structures displayed reversible deformations of approximately the same magnitude in each case.

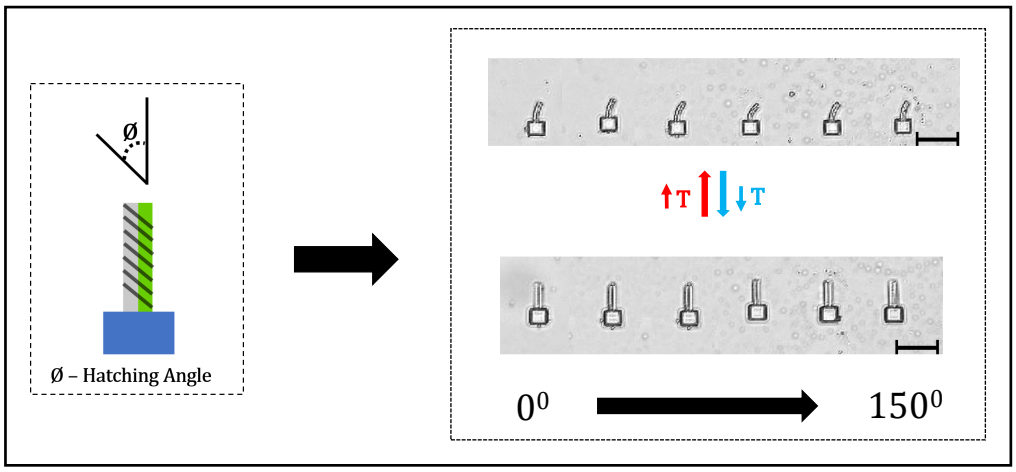


Fig. 31: Influence of hatching angle on the angular deformation of the beam. The hatching angle is increased from 0° to 150° in steps of 30° (Scale:50 µm)

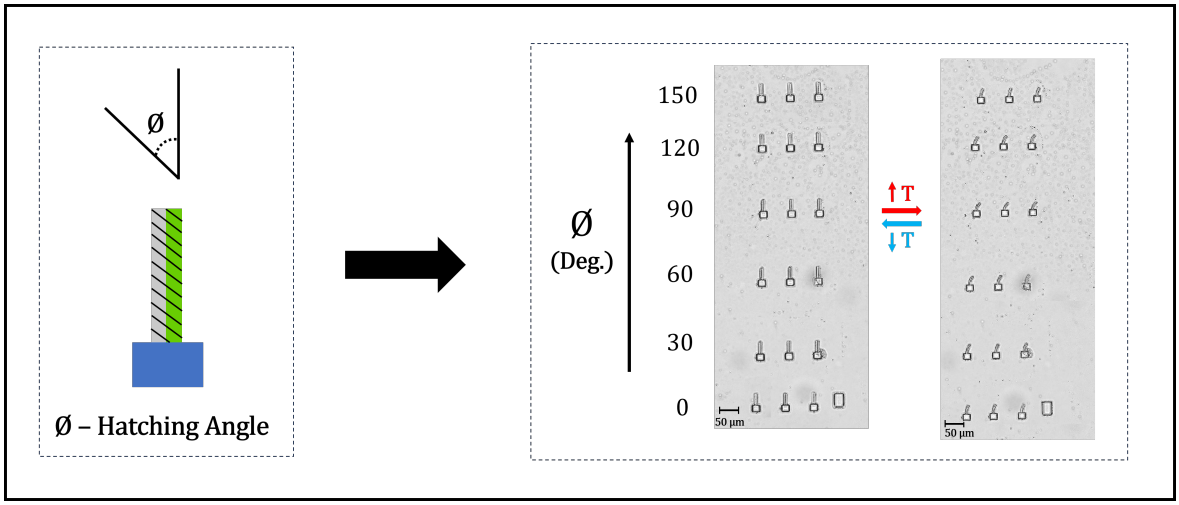


Fig. 32: Illustration of the sample set used to characterize the influence of hatching angle on beam deformations

Additional characterizations were also conducted where the two individual elements of the beam were printed using different hatching angles, as depicted in **Figure.33**.

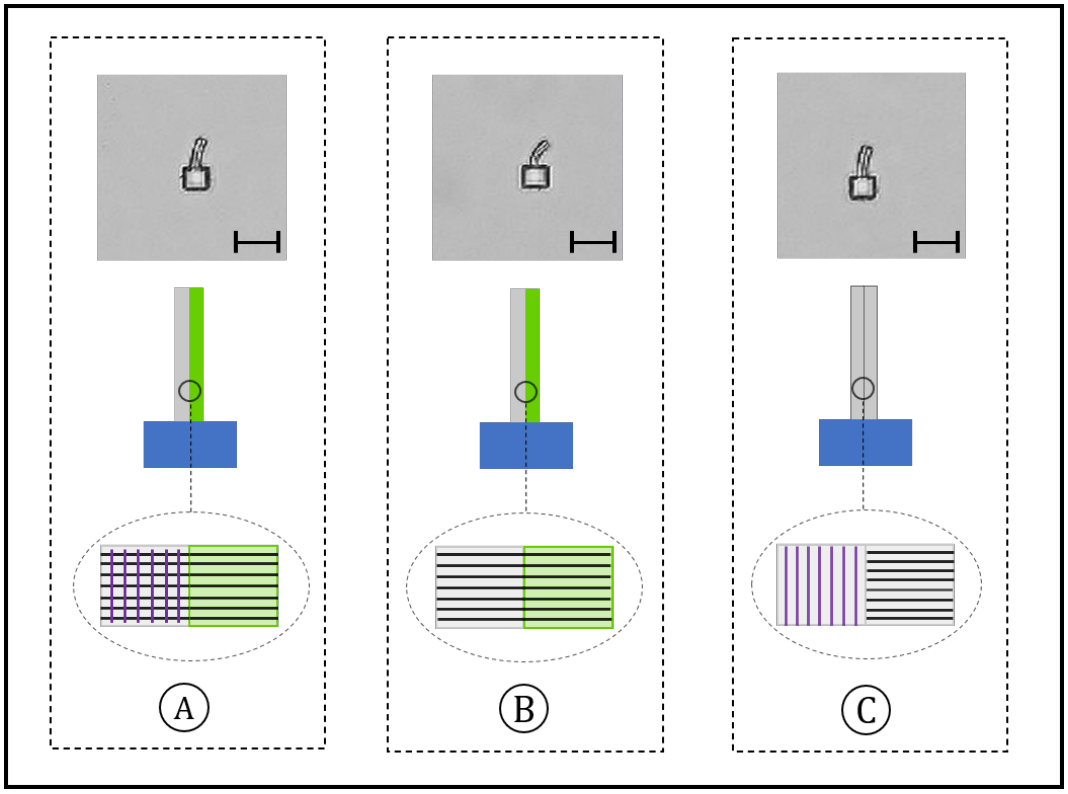


Fig. 33: Illustration of the influence of different hatching angles for each segment of the bi-layered beam on its angular deformation (Scale:50 µm)

In **case A** of **Figure.33**, the highly polymerized section of the beam comprises of layers in which successive slices comprise of hatch lines that are printed at an angle of 90° to one another. On the contrary, the lower polymerized section of the beam has all slices comprising of hatch lines oriented at an angle of 90° with respect to the vertical. When subjected to a thermal stimulus, the beam deforms to a smaller extent as compared to a beam in which all the hatch lines are inclined at an angle of 90° to the vertical **(Case B)**. Another test was performed in which both the layers of the bi-layered beam were printed

using the same printing parameters (laser power and scanning speed) but different hatching angles as shown in **Case C** of **Figure.33**. When subjected to thermal stimulus, the beam exhibits a directional response, thus indicating that hatching angle alone can be used to introduce the required heterogeneity in the structure to demonstrate a response to thermal stimulus.

### *R. Influence of Layer Width on Beam Deformation*

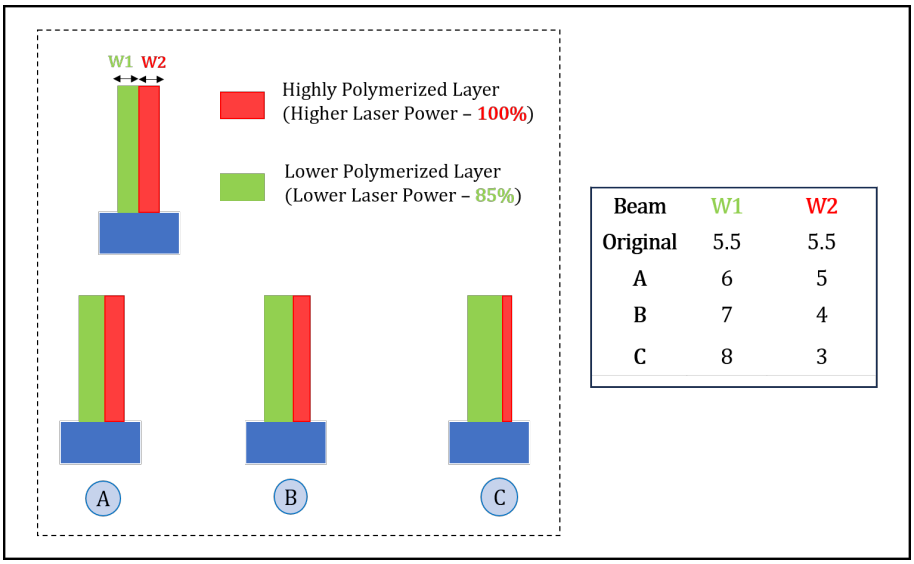


| Beam | W1 | W2 |
|---|---|---|
| Original | 5.5 | 5.5 |
| A | 6 | 5 |
| B | 7 | 4 |
| C | 8 | 3 |

Fig. 34: Illustration of the test performed to evaluate the influence of different layer thickness on the angular deformation of the beam

A test was performed to evaluate the impact of different layer thicknesses while characterizing the bi-layered beam model as discussed earlier in this paper. An illustration of this is as shown in **Figure.34**.

The width of the lower polymerized section of the bi-layered cantilever beam was systematically increased from 5.5 µm to 8 µm while the entire width of the bi-layered beam was maintained at 11 µm. When the beams were subjected to a temperature stimulus, delamination was observed between the layers of the beam (especially in Case B and C). One reason for this could be the small width of the highly polymerized section of the beam. Since the overall dimensions of the beam are small, further reducing the dimensions of the highly polymerized section of the beam resulted in this section not being printed as desired (resolution of 25x objective). Thus, a choice was made to maintain both layers of the beam at an equal width of 5.5 µm.

### *S. Evaluating Response of Beams to Different Solvents*

A study was conducted to evaluate the impact of the solvent used in the post-fabrication development of microstructures on the characteristics of the beam. Typically, either isopropanol or acetone is used for the development process. In this study, the microstructures were initially exposed to an isopropanol environment, and their behavior was recorded. Next, the same microstructures were exposed to an environment comprising of acetone, and their behavior was also recorded. The results obtained is as shown in **Figure.35**.

The results indicate that isopropanol induces deformation in the beam, with characteristics very similar to those observed when adding water at 60°C. However, the extent of shrinkage is minimal compared to the changes observed during thermal tests, and the deflection of the beam is not rapid as observed when the beam is subjected to a thermal stimulus. When the microstructures were subjected to an environment containing acetone, the structures did not show any deformation. Therefore, acetone was chosen for the development procedure as it would not induce any change in the geometry of the structure.

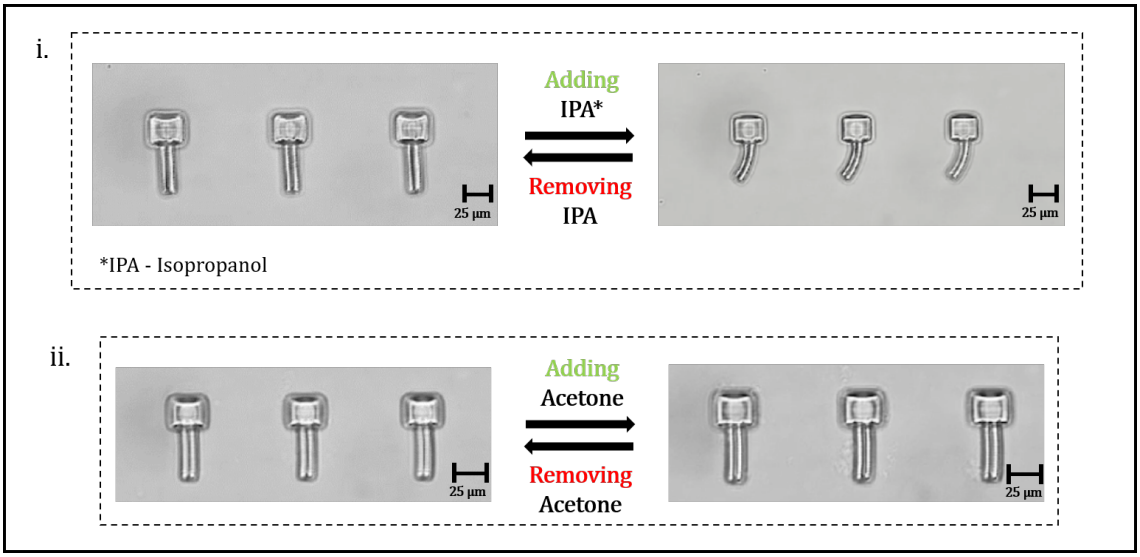


Fig. 35: Solvent-dependent deformation of microstructures

### *T. Evaluating Response of Beams to Change in pH*

A test was performed to determine if the hydrogel-based microstructures would respond to a change in pH. To achieve this, the beams were subjected to a pH of 2 by adding Acetic Acid (0.5 molar), and their deformation was evaluated. Next, the beams were subjected to a pH of 14 by adding NaOH solution (0.5 molar). An illustration of the test performed is as shown in **Figure.36**.

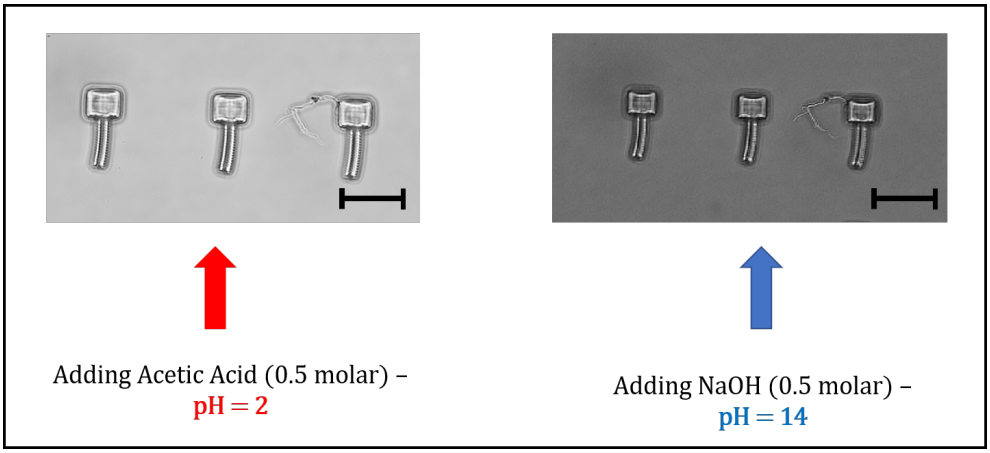


Fig. 36: Evaluating deformation in the beam when subjected to different pH levels (Scale: 50 µm)

The results obtained indicate that the hydrogel-based structure printed using the given composition of the photoresist is not sensitive to a change in pH. However, the pNIPAM-based hydrogel can be made sensitive to pH by incorporating acrylic acid chains within the hydrogel matrix, the details of which can be found in literature [49].

### U. *Overview of Poisson's Ratio*

Poisson's ratio is a way to characterize the deformation of a material in directions perpendicular to the direction in which a load is applied, as illustrated in **Figure.37**.

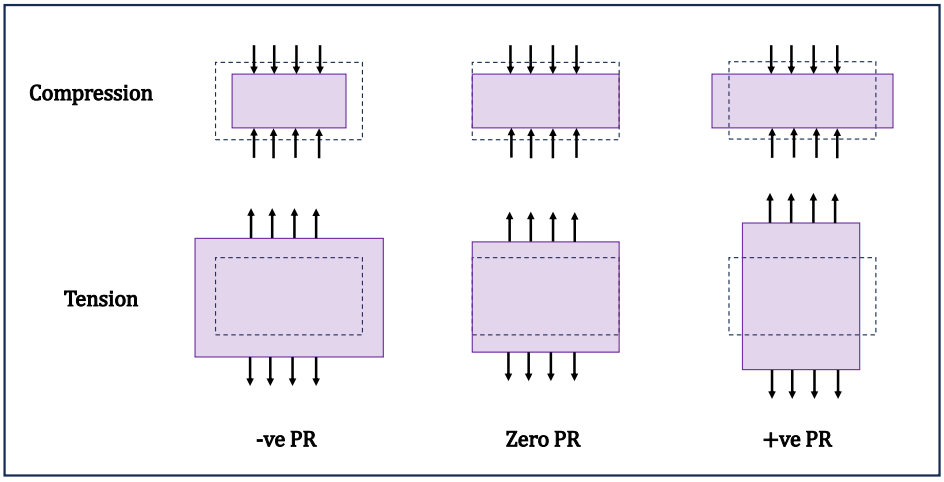


Fig. 37: Illustration of material deformation corresponding to different Poisson's ratios

Poisson's ratio is calculated using the expression provided below:

$$Poisson's\ Ratio = -\frac{Lateral\ Strain}{Longitudinal\ Strain} \tag{13}$$

The Poisson's ratio of an engineered structure largely depends on the design and configuration of the unit cells that make up the structure, as depicted in **Figure.38**.

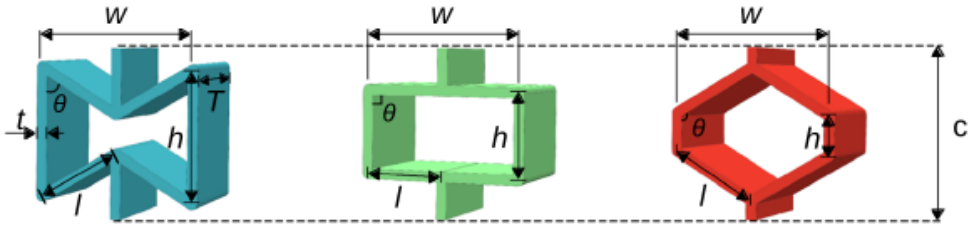


Fig. 38: Illustration of unit cells and their corresponding Poisson's ratio (PR). The unit cell on the left represents a geometry that exhibits a negative Poisson's ratio (auxetic unit cell). The unit cell in the middle represents a geometry that exhibits a near-zero Poisson's ratio while the unit cell on the right represents a unit cell that exhibits a large positive value of Poisson's ratio. The image is taken from literature [38]

It is to be noted here that the Poisson's ratio exhibited by these unit cell geometries is for small values of strain (typically in the range of 1% to 10%). In this thesis, emphasis is laid on geometries exhibiting a near-zero PR, and a positive PR.